RESEARCH ARTICLE

Robust Control of DFIG-Based WECS Integrating an Energy Storage System With Intelligent MPPT Under a Real Wind Profile

HAMID CHOJAA[1], AZIZ DEROUICH[1], OTHMANE ZAMZOUM[1], AZIZ WATIL[2],
MOHAMMED TAOUSSI[1], ALMOATAZ Y. ABDELAZIZ[3], (Senior Member, IEEE),
Z. M. S. ELBARBARY[4], AND MAHMOUD A. MOSSA[5]

[1]Industrial Technologies and Services Laboratory, Higher School of Technology, Sidi Mohamed Ben Abdellah University, Fez 30000, Morocco
[2]EEIS Laboratory, ENSET Mohammedia, Hassan II University of Casablanca, Casablanca 20650, Morocco
[3]Faculty of Engineering and Technology, Future University in Egypt, Cairo 11835, Egypt
[4]Department of Electrical Engineering, College of Engineering, King Khalid University, Abha 61421, Saudi Arabia
[5]Electrical Engineering Department, Faculty of Engineering, Minia University, Minia 61111, Egypt

Corresponding authors: Hamid Chojaa (hamid.chojaa@usmba.ac.ma) and Mahmoud A. Mossa (mahmoud_a_mossa@mu.edu.eg)

ABSTRACT This research work addresses the challenge of controlling a wind energy conversion system (WECS) connected to the grid, which incorporates a battery energy storage system and operates under varying real wind speed profiles. The system comprises a Doubly-Fed Induction Generator (DFIG) connected to the grid through an AC/DC/AC converter, along with a Li-ion battery pack storage unit linked to the Back-to-Back converter DC via a DC/DC converter. The study highlights that internal parametric variations and the non-linear behavior of the wind turbine negatively affect the energy quality produced, as well as the battery charging performance and its overall lifespan. To overcome these issues, the research proposes a robust control strategy based on Integral action Sliding Mode Control (ISMC) to independently manage the powers of the WECS, particularly the DFIG, to enhance dynamic performance. Furthermore, effective battery charging and discharging controllers are crucial for efficiently distributing the generated power to both the grid and the storage unit, ensuring proper energy extraction and battery charging/discharging. Depending on the battery's State of Charge (SOC), the available extracted energy, and the power injected into the grid, two current regulation modes are employed: buck charging mode and boost discharging mode. A storage system energy management algorithm is then utilized to determine the appropriate charging mode, ensuring battery safety. To validate the system's performance, a 1.5 MW wind power conversion system is tested using Matlab/Simulink simulations. The results demonstrate the robustness and efficiency of the proposed control approach in enhancing the overall system's performance.

INDEX TERMS Artificial neural network, DFIG, ISMC, MPPT technique, storage system, WECS.

I. INTRODUCTION

In response to climate change and the goal of achieving carbon neutrality [1], there is a noticeable global shift towards renewable energy. Numerous countries are actively working to increase the proportion of renewable energy in their electricity generation to combat global warming [2]. Notably, Morocco's commitment to mitigating climate change has

The associate editor coordinating the review of this manuscript and approving it for publication was Reinaldo Tonkoski.

earned it the eighth position in the 2022 Climate Change Performance Index. The country stands out as a leading force among nations striving to combat global warming [3]. Morocco is placing significant emphasis on advancing its renewable energy sector, with ambitious targets of surpassing a 52% share of renewable energy in the electricity mix and achieving 20% wind power in the energy mix by 2030 [4]. This focus on wind power aligns with the global recognition of wind energy as a crucial renewable resource due to its cleanliness, cost-effectiveness, sustainability, and

eco-friendliness [5]. The wind energy sector has experienced a surge in interest due to numerous advantages it offers, such as zero greenhouse gas emissions, continuous and abundant energy supply, and declining production costs, particularly with advancements in technology [6], [7]. Wind turbines are categorized into two types: horizontal axis and vertical axis wind turbines. Among these, horizontal axis wind turbines dominate the global landscape due to their superior power efficiency when compared to vertical axis wind turbines [10]. Recently, a novel type of turbine called the multi-rotor wind turbine has emerged as a potential replacement for traditional turbines [11]. These turbines have demonstrated highly satisfactory results in comparison to their conventional counterparts. The technology involves combining two or more turbines into one unit to enhance the mechanical energy harnessed from the wind [12]. This innovative approach has been extensively studied in various scientific works [13], [14], [15], [16]. Remarkably, the energy yield from wind using this new technology is 20% to 30% higher than what traditional turbines can achieve [17]. This technology offers several advantages over traditional turbines. One key benefit is its immunity to the wind interference that occurs between turbines in wind farms, ensuring enhanced durability [14], [15]. Moreover, adopting this technology leads to significant reductions in both the wind farm's physical footprint and implementation costs when compared to conventional turbines [13], [16]. However, it is worth noting that this technology comes with some drawbacks, such as its higher cost, complexity in control, and a considerable number of mechanical components [12], [14]. Central to the efficiency of this technology is the electric generator, which serves as the vital component responsible for converting the turbine's mechanical energy into electrical power. Various electric generator types can be used for this purpose, including asynchronous generators [18], synchronous generators [19], DC generators [20], and the doubly-fed induction generator (DFIG) [21]. Among these, the DFIG remains widely preferred, especially for variable wind speeds, due to its affordability, durability, ease of control, and low maintenance compared to other alternatives [22]. The wind energy generation system relies on diverse and numerous control strategies, which can be categorized into four distinct groups. The first group encompasses linear strategies like direct power control [23] and direct torque control [24]. These strategies stand out for their simplicity and ease of implementation, employing hysteresis comparators to regulate characteristic variables [25]. The second group comprises nonlinear strategies, such as sliding mode control (SMC) [26], synergetic control [27], backstepping control [28], high-order SMC [29], [30], and passivity control [31]. These approaches are more intricate than linear strategies and are tailored to the mathematical characteristics of the specific system under consideration. Their applicability extends to all electrical machines, encompassing electric motors and generators. Moving on to the third group, we encounter smart strategies,

including genetic algorithms [32], neural networks [33], particle swarm optimization [34], and fuzzy logic [35]. These strategies are employed to enhance the dynamic behavior and calculate system parameters. Their effectiveness in improving current quality surpasses that of classical strategies [33], [35]. The fourth group represents hybrid strategies, characterized by their remarkable efficiency compared to the other groups. Within this category, different or similar techniques are combined to significantly enhance system durability. Examples of such hybrid strategies include synergetic-SMC [36], backstepping-SMC [37], synergetic-super twisting algorithm [38], neuro-SMC [39], Fuzzy-SMC [40], and neural DPC [41], among others.

One of the most pressing current issues is the generation and transmission of electrical energy produced by wind energy in isolated or remote areas where transmission lines cannot be used. Furthermore, wind energy is known to be random in nature, as the resulting electrical energy is dependent on climate conditions and weather. In order to solve this problem and provide isolated and remote areas with energy during24/24 hours, storing electrical energy using energy storage systems is mandatory and crucial [42]. Storing electric energy is completely different from generating it, and take a significant importance as a research topic in the industrial field.

Electric energy storage has been dealt with in several research topics [43], [44], [45], [46], [47], [48], where the focus has been on the control aspect and giving the mathematical shape to the battery. The latter is a necessary and effective task in the process of storing electrical energy. Recently, much focus has been placed on the battery in terms of manufacturing, controlling and protecting it from external and internal risks. The battery is used typicallyin the electric car and makes up approximately 90% of the total weight of thesystemelectric car [49]. It is also the most substantial component. Lithium, nickel-cadmium, and lead-acid batteries are the most common used technologies, with lithium-ion batteries having the highest energy density, specific energy, and voltage cell [50]. This type of battery is pollution-free and has a low self-discharge rate and a long life. Several research works have been carried out on batteries, which dealt with giving the mathematical shape of the battery, controlling the battery charge, estimating the battery parameters, and protecting itagainst risks using neural networks [51], the extended Kalman filter (EKF) [52], fuzzy logic [53], and the unscented Kalman filter [54]. Using these strategies requires a large amount of data experimentation, long-term calculations, and a learning algorithm to achieve a reliable estimation of the battery terminals voltage.

In the field of wind energy using a DFIG generator, a DC-DC inverter is used to charge optimally the battery and thus store energy [55], as this inverter needs a highly efficient control strategy. To control this inverter, we can use linear strategies, non-linear strategies, smart strategies, and hybrid strategies, where the use of these strategies depends on the

degree of simplification and complexity of the system, the cost of the system and the extent of its protection. As is well known, the higher degree of complexity and protection is, the higher becomes the overall cost of the system, which is undesirable. To generate the control pulses of the battery charge inverter both pulse width modulation (PWM) [56] and space vector modulation (SVM) [57] can be used. Also, neural PWM [58], neural SVM [59], and modified SVM [60] can be adopted to generate control pulses for the battery charge inverter because of the advantages and results offered by these strategies. Frequent variations in load demand and unfavorable weather conditions reduce battery charging performance and decrease its effectiveness over time. Therefore, it is necessary to balance the energy of wind turbines to the direct current load and the battery immediately, and this is done by proposing a control strategy with very high efficiency and effectiveness. In addition, one must focus on the total cost of the system and the quality of the electric current, as well as the extent to which the battery is protected from internal and external risks. Also, looking for the easiest and fastest way to charge the battery is very important. The type of DC-DC converter used in charging the battery increases the complexity of the system and its cost, as it is necessary to choose a converter that is characterized by ease of control and programming [61]. For this purpose and in order to manage the battery charge, an algorithm is proposed as a safeguard smooth switching between various operational modes, while achieving a suitable charging position for the batteryandthus ensuring a longer battery life.

In this research study, a nonlinear robust control strategy is proposed for a WECS based on DFIG, involving a battery energy storage system. Maximum wind energy extraction is achieved by operating the WECS in variable speed mode with an ANN speed controller. Then, multi-loop nonlinear ISMC are developed to ensure efficient and robust control of the DFIG's powers with minimal chattering caused by discontinuous control, allowing simultaneous capture of maximum wind power with fluctuating wind speed and power quality improvement by canceling the utility grid's most significant harmonics. Moreover, to overcome the problem of the intermittent nature of wind power, the grid power fluctuation is handled, as well as the deal with the safety of the battery during the charging or discharging conditions. Unlike all previous works where the injected grid power varies in view of the wind fluctuation which can provide degradation of the stability of the grid network, the main contribution in this work is to use a storage system to maintain a constant injected power in the grid, by smoothing out the extracted wind power fluctuations through storing the excess of energy during times of high wind and releasing the stored energy during times of low wind, thus providing a more stable and consistent behavior to the grid. As well as to deal with the safety of the battery during the charging or discharging process, a DC/DC power electronic interface is placed between the DC link voltage and the storage unit, which can regulate the power flow during the charging or discharging mode, thus increase the battery lifetime and guarantee the safety of the battery.

The research aims to achieve the following objectives:

1. Develop a reliable and efficient controller design for the Doubly-Fed Induction Generator (DFIG) to address chattering issues caused by discontinuous control, ensuring precise control over active and reactive power.

2. Validate the effectiveness of the proposed DFIG controller using real wind speed profiles, assessing performance metrics such as steady state error, active power, reactive power, torque ripples reduction, and mitigation of Total Harmonic Distortion (THD) in grid currents.

3. Create an effective Maximum Power Point Tracking (MPPT) technique with an artificial neural network speed controller. This intelligent controller utilizes mechanical speed measurements to deliver accurate electromagnetic torque control signals to the DFIG.

4. Implement a storage system that stabilizes grid power by storing excess wind energy during high wind periods and releasing it during low wind periods. This ensures a consistent output from the system.

The rest of this work is organized as follows: Section II goes over the WECS mathematical modeling, which includes the wind turbine model, the GSPC and RSPC models, as well as the storage system description and modeling. Section III is devoted to system control and includes the MPPT technique control, RSPC control, GSPC control, battery energy storage system control, and battery management Algorithm. Section IV presents the simulation results of a 1.5 MW DFIG-based WECS with a real wind speed profile of Tetouan city in Morocco. Finally, this research work is concluded with the key points deriving from it and perspectives.

II. PROPOSED SYSTEM

Figure 1 depicts the entire system that will be studied, which consists of a wind energy conversion system using doubly-fed induction generator and an energy storage system using batteries. Our goal is to model and simulate a wind turbine with a DFIG and to ensure independent control of reactive and active power by a robust ISMC method, with an intelligent MPPT technique based an ANN for maximum efficiency of wind to electricity conversion, all associated with a storage unit to help keep the power produced to the grid as constant as possible.

The system to be modeled consists of the mechanical part of the wind turbine, the generator with the inverter connected to the rotor and its control, the rectifier that feeds the DC bus, the energy storage system and the electrical grid to which the wind energy conversion system is connected.

It is important to keep in mind that our goal is to study the global functioning of the whole system in order to optimize the wind power production to allow an easier management and insertion of this one in the electrical grid. For these reasons, we will simplify the modeling of the different elements in order to keep a system allowing a suitable implementation
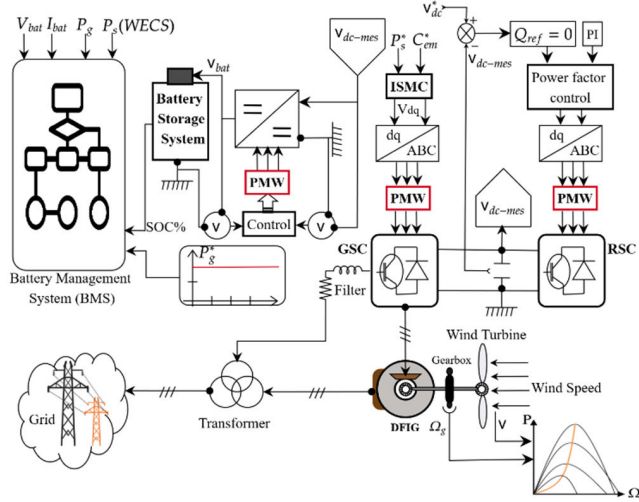
FIGURE 1. Proposed system.

FIGURE 2. Power Coefficient C$_p$ (λ, β) as function of TSR λ and β. (a) 2D plot, (b) Surface plot.

on the simulation software and to perform simulations with reasonable computation times.

A. WIND TURBINE MODEL

The turbine is one of the means that was invented in the last century in order to generate electrical energy from wind and water energy. The wind energy is converted into mechanical energy by this turbine [62], [63], [64]. The latter is used to turn the electric generator. The wind turbine is a structure, where three or two blades can be used. Wind turbines that use three blades are the most widely used on land and sea [65]. The power and torque produced by a wind turbine can be written in the form of the following equations [66]:

$$P_t = \frac{1}{2}\rho \pi R^2 V^3 C_P(\lambda, \beta) \quad (1)$$

$$T_{aer} = \frac{1}{2\Omega_t}\rho \pi R^2 V^3 C_P(\lambda, \beta) \quad (2)$$

where, T$_{aer}$ is the aerodynamique torque, ρ is the air density, R is the blade length, V is the wind speed, P$_t$ is the total power generated turbine, and *Cp* is the power coefficient.

In the wind turbine, there is a coefficient called power coefficient that is of great importance in calculating the power generated by the turbine, as the largest value it takes is 0.59 and its value is related to the angle of the turbine blades facing the wind. Equation (3) represents the power coefficient of the studied wind turbine.

$$Cp(\lambda, \beta) = 0.5\left(\frac{116}{\lambda i} - 0.4\beta - 5\right)exp\left(\frac{-21}{\lambda i}\right) + 0.0068\lambda \quad (3)$$

There is another parameter in the wind turbine that is no less important than the power coefficient called the TSR, as it is used to determine the maximum value of the power gained from the wind [67]. Equation (5) describes the TSR of wind

turbine used in this paper.

$$\frac{1}{\lambda i} = \frac{1}{\lambda + 0.08\beta} - \frac{0.035}{\beta^3 + 1} \quad (4)$$

With:

$$\lambda = \frac{\Omega_t R}{V} \quad (5)$$

Figure 2 illustrates the Cp (λ, β) coefficient curves given by equation (3) [41]. Its maximum value (Cp (λ, β) max=0.4798) is reached for $\beta = 0°$ and $\lambda_{opt} = 8.124$.

Equation (6) represents the relationship between the torque and speed of the turbine and the relation betweenthose of the electric generator, where the torque of the turbine is greater than that of the electric generator. However, the speed of the electric generator is higher than that of the turbine.

$$\begin{cases} T_m = \dfrac{T_{aer}}{G} \\ \Omega_m = G\Omega_t \end{cases} \quad (6)$$

where, T_m and Ω_m are the torque and the speed on the gearbox high-speed shaft (generator side), G is the gearbox ratio.

Equation (7) represents the mechanical part modelof the turbine-generator system, whereby this equation controls the operation of the electric machine as a motor or electric generator.

$$J\frac{d\Omega_m}{dt} = C_m - T_{em} - f.\Omega_m \quad (7)$$

where, T_{em} is the torque produced by DFIG.

The MPPT technique is adopted and presented in the following section, in order to ensure the extraction of the maximum power available in the wind.

B. DFIG MODEL

In the field of wind power generation, DFIG is the beating heart of this system, as it is responsible for converting mechanical energy into electrical energy. This generator is frequently used in the case of variable wind speed. It is necessary to give the mathematical form to this generator using the Park transformation. The global mathematical equations of the active/reactive powers, voltages and flux of the DFIG in the Park reference are defined as follows [62], [63]:

Stator and rotor voltages equations:

$$
\begin{cases}
V_{sd} = R_s i_{sd} + \dfrac{d}{dt}\phi_{sd} - \omega_s \phi_{sq} \\
V_{sq} = R_s i_{sq} + \dfrac{d}{dt}\phi_{sq} + \omega_s \phi_{sd} \\
V_{rd} = R_r i_{rd} + \dfrac{d}{dt}\phi_{rd} - (\omega_s - \omega_r)\,\phi_{rq} \\
V_{rq} = R_r i_{rq} + \dfrac{d}{dt}\phi_{rq} + (\omega_s - \omega_r)\,\phi_{rd}
\end{cases}
\tag{8}
$$

where: ω_s, ω_r, R_s and R_r denote stator pulsation, rotor pulsation, stator resistance, and rotor resistance respectively.

Stator and rotor flux equations:

$$
\begin{cases}
\phi_{sd} = L_s i_{sd} + L_m i_{rd} \\
\phi_{sq} = L_s i_{sq} + L_m i_{rq} \\
\phi_{rd} = L_r i_{rd} + L_m i_{sd} \\
\phi_{sq} = L_r i_{rq} + L_m i_{sq}
\end{cases}
\tag{9}
$$

where, L_r and L_s is the inductance of the rotor and stator, i_{rd} and i_{rq} are the rotor currents, $\phi_{rd}, \phi_{rq}, \phi_{sd}$ and ϕ_{sq} are the rotor and stator fluxes, L_m is the mutual inductance.

Active and Reactive powers equations:

$$
\begin{cases}
P_s = \dfrac{3}{2}Re\left\{\vec{V}_s \times \vec{I}_s^*\right\} = \dfrac{3}{2}\left(V_{sd}i_{sd} + V_{sq}i_{sq}\right) \\
Q_s = \dfrac{3}{2}Im\left\{\vec{V}_s \times \vec{I}_s^*\right\} = \dfrac{3}{2}\left(V_{sq}i_{sd} - V_{sd}i_{sq}\right)
\end{cases}
\tag{10}
$$

The electromagnetic torque is expressed as:

$$
\Psi T_{em} = \frac{3}{2}p\frac{L_m}{L_s}Im\left\{\vec{s} \times \vec{I}_r^*\right\} = \frac{3}{2}p\frac{L_m}{L_s}\left(\phi_{sq}i_{rd} - \phi_{sd}i_{rq}\right)
\tag{11}
$$

where, p is the number of pole pairs.

C. GRID SIDE INDUCTIVE FILTER MODEL

Once the converter with two level topology has been analyzed, the inductive filter which is located between the GSPC outputs and the grid voltage is presented next. This filter is normally constituted by three equivalent and independent inductances in series with resistance as illustrated in Figure 3. The sub-index "f" represents the output AC voltages of the GSPC. The grid supply is modeled by three phase sinusoidal voltages generated at constant frequency and amplitude [67].

Thus, the mathematical model of this system can easily be obtained using the following electrical equations:

$$
\frac{di_{ag}}{dt} = \frac{1}{L_f}\left(v_{af} - R_f i_{ag} - v_{ag}\right)
\tag{12}
$$

$$
\frac{di_{bg}}{dt} = \frac{1}{L_f}\left(v_{bf} - R_f i_{bg} - v_{bg}\right)
\tag{13}
$$

$$
\frac{di_{cg}}{dt} = \frac{1}{L_f}\left(v_{cf} - R_f i_{cg} - v_{cg}\right)
\tag{14}
$$

where v_{af}, v_{bf}, v_{cf} are the output voltages of the GSPC, v_{ag}, v_{bg} and v_{cg} are the grid voltages and i_{ag}, i_{bg} and i_{cg} are the currents flowing thorough the inductive filter.
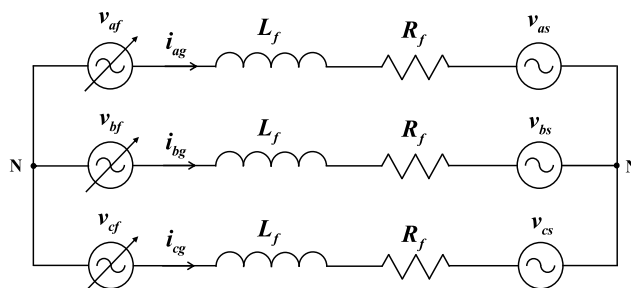

FIGURE 3. Simplified representation of the grid side circuit.

Therefore, the decomposition of each magnitudes into d and q components yield the expressions below:

$$
\frac{di_{gd}}{dt} = \frac{1}{L_f}\left(v_{fd} - R_f i_{gd} - v_{gd} + \omega_s L_f i_{gq}\right)
\tag{15}
$$

$$
\frac{di_{gq}}{dt} = \frac{1}{L_f}\left(v_{fq} - R_f i_{gq} - v_{gq} - \omega_s L_f i_{gd}\right)
\tag{16}
$$

The DC linkage between the RSPC and GSPC is achieved by a capacitor (or combination of capacitors). It tries to keep a constant voltage in its terminals thanks to the energy stored within it. The DC link model is derived using the capacitor voltage [41], [78]:

$$
U_{dc} = \frac{1}{C}\int i_{dc}dt
\tag{17}
$$

where C is the DC link capacitance. The current idc through the capacitor can be denoted as:

$$
i_{dc} = i_{r\_cc} - i_{g\_cc}
\tag{18}
$$

where i_{r_cc} is the current flowing from RSPC and i_{g_cc} is the current flowing to the GSPC.

The injected active and reactive powers in the grid can be expressed as:

$$
P_g = \frac{3}{2}v_{gd}i_{gd} = \frac{3}{2}v_g i_{gd}
\tag{19}
$$

$$
Q_g = -\frac{3}{2}v_{gd}i_{gq} = -\frac{3}{2}v_g i_{gq}
\tag{20}
$$

D. STORAGE SYSTEM DESCRIPTION AND MODELING

1) SYSTEM PRESENTATION

A storage unit is a system that uses rechargeable batteries to store electrical energy and provide backup power during blackouts [42]. A storage unit can help to mitigate the effects of fluctuations in the power output of a WECS (Figure 4), which improves the overall system efficiency, increases energy reliability, and improves the stability of the electrical grid. The storage unit typically consists of a power electronic device that manages the electrical power flow, as well as a battery energy storage system (BESS) which is primarily made up of battery packs [68].
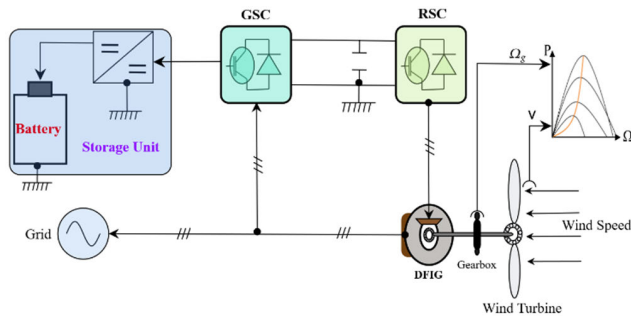
FIGURE 4. Wind energy generation combined with a storage system.

The battery energy storage unit, object of our study, is illustrated by Figure 5. It is made up of a series of bidirectional buck boost power converters and battery energy storage composed of Li-ion batteries packs. To help improve the overall performance and efficiency of the battery charging/discharging process, an LC filter consists of an inductor (L) and a capacitor (C) is placed between the DC/DC converter and the storage unit.
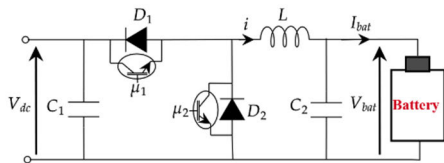
FIGURE 5. Schematic diagram of the DC/DC converter with the battery pack.

2) MODELING OF THE ASSOCIATION DC/DC CONVERTER WITH THE BATTERY PACK

The buck boost converter is selected as the sole power electronic interface between the Li-ion battery Pack and the DC bus voltage. This converter can operate in either buck or boost mode depending on the power flow direction. The buck mode ensures an adequate battery charging mode while the boost mode guarantees the safety of the battery discharging mode.

The switching signals μ_1, μ_2 are generated by a PWM circuit and take values in the finite set {0, 1}. To design a

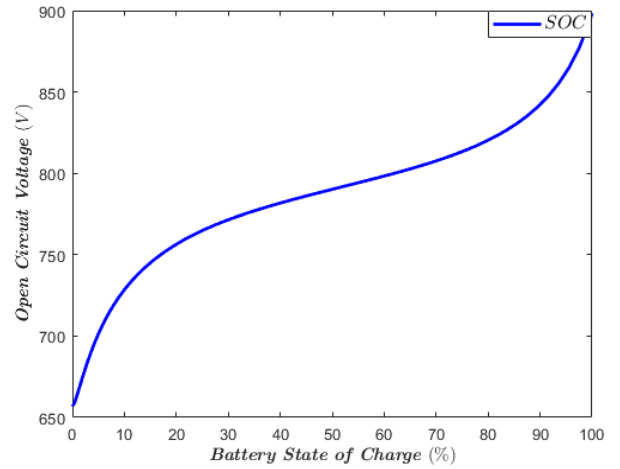Battery charger controller, the first step is to elaborate an accurate model describing the studied system dynamics.

FIGURE 6. Open circuit voltage of the battery U_{ocv}.

In this work, we consider the battery electrical model composed by a series combination of a resistance and a voltage source, where the internal resistance of the battery characterize the battery energy losses and the internal battery voltage refers to open circuit voltage Uocv, which varies nonlinearly with the SoC (%) of the battery ($U_{ocv} = f$ (SoC)) [69], [70], as illustrated in Figure 6.
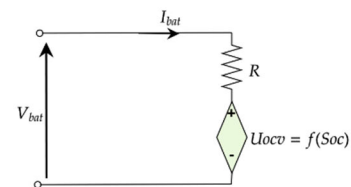

FIGURE 7. Model of a battery equivalent circuit.

When Kirchhoff's laws are applied to the association of a DC-DC converter with the equivalent circuit of the battery shown in Fig. 7, the following differential equations are obtained:

$$L\frac{di}{dt} = \mu V_{dc} - V_{bat} \tag{21}$$

$$C\frac{dV_{bat}}{dt} = i - I_{bat} \tag{22}$$

$$I_{bat} = \frac{V_{bat} - U_{ocv}}{R_b} \tag{23}$$

$$U_{ocv} = f(SOC) \tag{24}$$

where, V_{dc}, V_{bat}, i and I_{bat}, denote respectively, the DC-bus voltage, the batteryvoltage, the inductor current and the battery current; R_b is the battery internal resistor. The PWM input control signal μ is expressed as follows:

$$\mu = S\mu_1 + (1 - S)(1 - \mu_2) \tag{25}$$

With, the switching variable S which defines the two operating modes of the studied bidirectional battery charger (S = 1 Buck mode and S = 0 in Boost mode).

3) STORAGE CAPACITY

The power used to size the storage unit is roughly equal to the power extracted from the generator by removing the stable power supplied to the network $P_g = 0.8$ MW:

$$P_B = P_s - P_g \tag{26}$$

Now that we've determined the nominal storage power, we need to determine the energy capacity of the storage unit. To do so, we'll track the energy W_{stored} that needs to be stored or destocked by integrating the power that corresponds to storage over time:

$$W_{stored} = \int P_B dt \tag{27}$$

III. SYSTEM CONTROL

A. MPPT TECHNIQUE

The MPPT method allows adjusting the electromagnetic torque so that it can force the generator speed to reach its reference. For a given operating point, the maximum power extracted can be achieved only if the aerodynamic power coefficient $C_p(\lambda, \beta)$ achieves its maximum value. Moreover, this can be done when the TSR λ reaches its optimum value λ_{opt} [62]. Therefore, the reference generator speed Ω_{gref} is given by the following equation:

$$\Omega_g^* = G \frac{\lambda_{opt}}{R} V \tag{28}$$
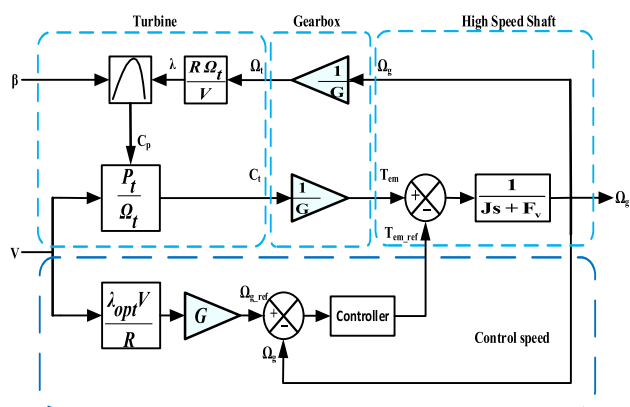
FIGURE 8. MPPT method.

Figure 8 represents the structure of the proposed MPPT method, where the mechanical speed is commanded by the electromagnetic torque reference T_{em_ref}. In addition, the MPPT strategy is used to compute the reference value of P_s.

The architectural scheme of the proposed MPPT neural network controller is shown in Figure 9. A two-layer network with a total of 15 neurons is used to implement the rotational speed controller. This neural controller is made up of two
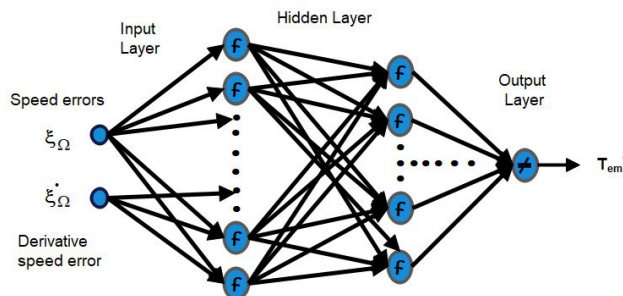
FIGURE 9. Internal structure of the ANN controller.

TABLE 1. Optimal specifications of the proposed ANN model of the speed regulator.

ANN Parameters	Value/Methods
	ANN- ξ_Ω
Training algorithm	Backpropagation
Process of MLP training	algorithm of Levenberg Marquardt
Suggested structure	2-15-1-1
Iterations number	1000
Layer of entry (2 neurons)	ξ_Ω, $\dot{\xi}_\Omega$
Output layer (one neuron)	T_{em_ref}
Activation functions	Tansig
Adaption learning function	Trainlm

neurons that represent the rotational speed error in the input layer and its derivative successively, a hidden layer and an output layer with one neuron representing the reference electromagnetic torque [58]. Table 1 presents the parameters of the artificial neural network controller used in this work.

After the training is finished, the algorithm's information is used to analyze the results. Figure 10 illustrates the architecture used as well as the analysis parameters and performance. Several tests for the mechanical speed of rotation data are performed until the higher regression R value conditions of training, low Mean Squared Error MSE, validation, and testing are reached, as illustrated in Figures 10 and 11. The network's performance function is represented by the MSE. When MSE is small, it indicates the training set's desired outputs have become very close to each other. The performance diagram of the mechanical speed data is depicted in Figure 11. The performance characteristics show the graph of error versus epochs for validation, training and test performance of the training records. Typically, after several training epochs, the error decreases on the validation data set as the network begins to overfit the training data. In the default configuration, after 1000 epochs, the training is terminated, and the best performance with the lowest validation error is extracted. We note from the Figure 11 that our proposed structure (2-15-1-1) converge quickly to the best value after 1000 epochs, with a best error variation achieving 4.0895×10^{-4}.
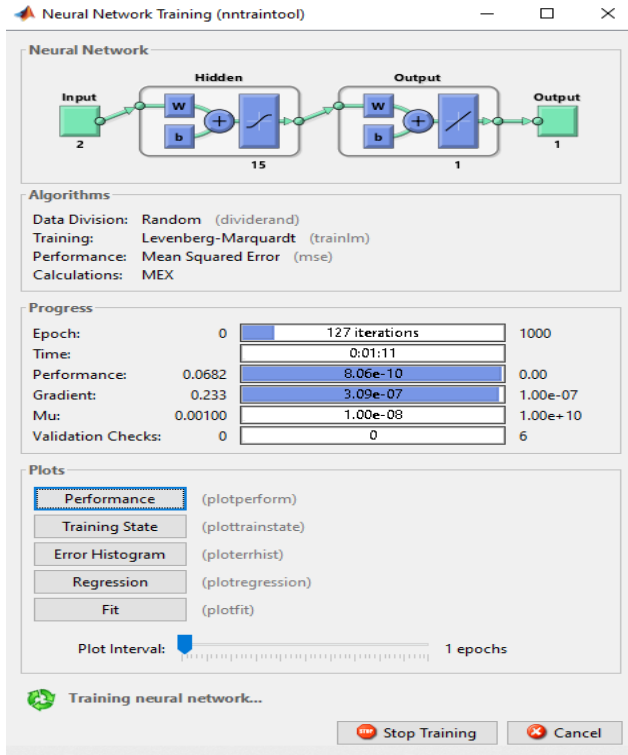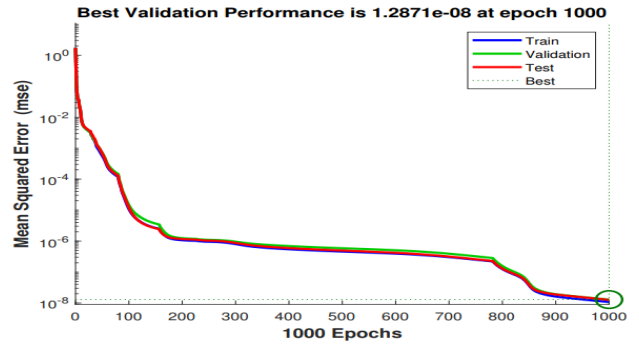
FIGURE 10. ANN learning progress.

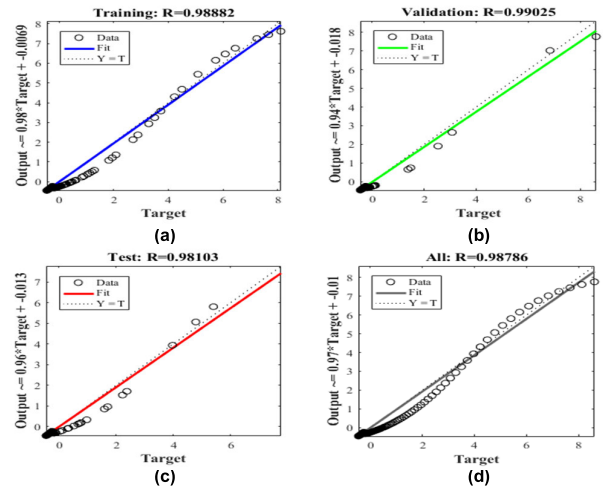FIGURE 11. Performance diagram of training.

FIGURE 12. Data regression analysis between the network response and the desired objectives: (a) Training: R=0.98882, (b) Validation: R=0.99025, (c) Test: R=0.98103, and (d) Overall: R=0.98786.

Figure 12 depicts the regression plot for phase a data as well as the regression values in training, validation, and test cases. Then, in order to check how well the input and output data are fitted in the network, the regression plot is used. 70% of the data is used for training, 15% of the data is used for validation, and 15% of the data is used to test the network. The regression graphic contains four graphics for training, testing, validation and the combination of all. The neural network's training curve can be compared to the best training algorithm. Figure 12 depicts the data regression analysis between network response and desired goals. The value of R denotes the correlation coefficient between the outputs and the objectives. Because all parameters (regression R) are very close to 1, the correlation between the outputs and the targets is very high. The data falls along a 45 degree line, as shown in the regression graph. It satisfies the requirement that the data be perfectly fitted.

B. ISMC TECHNIQUE OF RSPC

SMC is a type of non-linear strategy that has proven effective in improving the performance and effectiveness of systems. This strategy is highly efficient in improving current quality in wind systems, where durability is one of its main advantages [71]. In the case of changing system parameters, the SMC strategy is not much affected compared to linear strategies such as field-oriented control [62]. The negative side of this strategy is the existence of a chattering problem that limits its use [26]. This problem is due to the use of a discontinuous part in the SMC [72]. Several scientific works have been proposed in order to overcome this problem, where fuzzy logic [73], neuro-fuzzy algorithm [74], and neural networks [39] have been used. Among other solutions that have been proposed are super twisting algorithm [75] and third-order sliding mode control [76], [77]. However, there is a proposal that was discussed in [78] that proved its effectiveness in overcoming the defects and problems of the traditional strategy. This derivative is called Integral sliding mode control (ISMC). This strategy has proven its effectiveness in overcoming the defects of the traditional strategy and in improving the quality of the current. Also, minimizing active and reactive power ripples [78].

The sliding mode control method is divided into two parts, a first (continuous part) for the exact linearization, called the equivalent command U_{eq}, and a second (discontinuous component) for the stabilization, called the switching command U_n.

$$U = U_{eq} + U_n \qquad (29)$$

For a non-linear system presented in the following form:

$$\dot{x} = f(x, t) + g(x, t) U(x, t); \quad x \in R^n; \quad U \in R \qquad (30)$$

where: $f(x, t)$, $g(x, t)$ are two continuous and uncertain non-linear functions, described in our case as follows (31) and (32), as shown at the bottom of the page, with, $X = \begin{bmatrix} i_{rd} & i_{rq} \end{bmatrix}$

After simplification, equation (31) becomes:

$$f(x, t) = \begin{bmatrix} f_1 \\ f_2 \end{bmatrix}$$
$$= \begin{bmatrix} -\frac{R_r}{(\sigma L_r)^2}\left(\sigma L_r i_{rd} + \frac{MV_s}{\omega_s L_s}\right) + \frac{R_r M \psi_s}{L_s (\sigma L_r)^2} + \omega_r i_{rq} \\ -\frac{R_r}{\sigma L_r} i_{rq} - \frac{\omega_r}{\sigma L_r}\left(\sigma L_r i_{rd} + \frac{M}{\omega_s L_s} V_{sq}\right) \end{bmatrix}$$

(33)

where:

$$\begin{cases} \psi_{sd} = \psi_s; \psi_{sq} = 0 \\ V_{sd} = V_s = \omega_s \Psi_s; V_{sq} = 0 \end{cases}$$

(34)

The sliding surface, corresponding to the integral action sliding mode control theory, can be expressed as follows:

$$S(t) = \left(\frac{d}{dt} + \lambda_s\right)^{n-1} e(t) + K_i \int_0^\infty e(t)\, dt; e(t) = x^d - x^*$$

(35)

where $e(t)$ represents the difference between the desired signal x^d and the reference x^*. λ_s and n are the positive coefficient and the relative degree respectively.

The control by the ISMC technique contains an additional integral action to the conventional SMC technique to confront the chattering phenomenon caused by the discontinuous command signal.

In this work, the sliding surface is expressed in the following equation.

$$S(t) = e(t) + K_i \int_0^\infty e(t)\, dt$$

(36)

It is well known that the active and reactive stator powers are directly related to the quadrature and direct components of the rotor currents. The following equation expresses the error function between the measured and the reference rotor currents.

$$\begin{cases} e_d = I_{rd}^* - I_{rd} \\ e_q = I_{rq}^* - I_{rq} \end{cases}$$

(37)

By deriving the sliding surfaces, we find.

$$\begin{cases} \dot{S}(I_{rd}) = \dot{I}_{rd}^* - \left(\frac{V_{rd}}{\sigma L_r} - \frac{R_r}{\sigma L_r} i_{rd} + (\omega_s - \omega_r) i_{rq} + K_i e\right) \\ \dot{S}(I_{rq}) = \dot{I}_{rq}^* - \left(\frac{V_{rq}}{\sigma L_r} - \frac{R_r}{\sigma L_r} i_{rq} - (\omega_s - \omega_r)\right. \\ \left. \left(\frac{M}{\sigma L_r L_s}\phi_s + i_{rd}\right) + K_i e\right) \end{cases}$$

(38)

The equivalents control components V_{rdq}^{eq} can deduced from the previous equations and written as:

$$\begin{cases} V_{rd}^{eq} = \sigma L_r \dot{I}_{rd}^* + R_r i_{rd} - (\omega_s - \omega_r) i_{rq} \sigma L_r - K_i e \\ V_{rd}^{eq} = \sigma L_r \dot{I}_{rq}^* + R_r i_{rq} + (\omega_s - \omega_r)\left(\frac{M}{L_s}\phi_s + \sigma L_r i_{rd}\right) - K_i e \end{cases}$$

(39)

The Lyapunov function, which ensures the SMC's stability, is described as:

$$V = \frac{1}{2} S^2$$

(40)

To ensure Lyapunov function convergence, the derivative of Eq. (40) must be negative:

$$\dot{V} = S\dot{S} = S(\dot{e} + K_i e) < 0$$

(41)

The switching commands goal is to examine the attractiveness conditions. As a result, the discontinuous component is defined by the following equation:

$$U_n = \varepsilon Sat(e(t) + K_i \int_0^\infty e(t)\, dt)$$

(42)

C. CONTROL TECHNIQUE FOR GSPC

The GSPC's control goal is to stabilize the DC link voltage and set the filter's reactive power to zero. As illustrated in Figure 13, The DC bus link will be controlled in two steps by two PI controllers. The first PI controller calculates the DC link reference voltage value that brings the bus voltage to its reference value. The current reference value is then sent to the internal control loop, where the second PI controller is programmed to track this reference input via the filter's direct current component [63], [67].

D. CONTROLLERS DESIGN FOR BATTERY ENERGY STORAGE SYSTEM

1) BUCK CHARGING MODE

This mode provides an accurate battery current regulation during the battery charging mode. The battery current must be

$$f(x, t) = \begin{bmatrix} -\frac{R_r}{(\sigma L_r)^2}\left(\sigma L_r i_{rd} + \frac{MV_{sq}}{\omega_s L_S}\right) + \frac{R_r M \psi_{sd}}{L_S (\sigma L_r)^2} + \frac{\omega_r}{\sigma L_r}\left(\sigma L_r i_{rq} + \frac{M}{\omega_s L_s} V_{sd}\right) \\ -\frac{R_r}{(\sigma L_r)^2}\left(\sigma L_r i_{rq} + \frac{MV_{sd}}{\omega_s L_s}\right) + \frac{R_r M \psi_{sq}}{L_s (\sigma L_r)^2} + \frac{\omega_r}{\sigma L_r}\left(\sigma L_r i_{rd} + \frac{M}{\omega_s L_s} V_{sq}\right) \end{bmatrix}$$

(31)

$$g(x, t) = \begin{bmatrix} \frac{1}{\sigma L_r} & 0 \\ 0 & \frac{1}{\sigma L_r} \end{bmatrix}$$
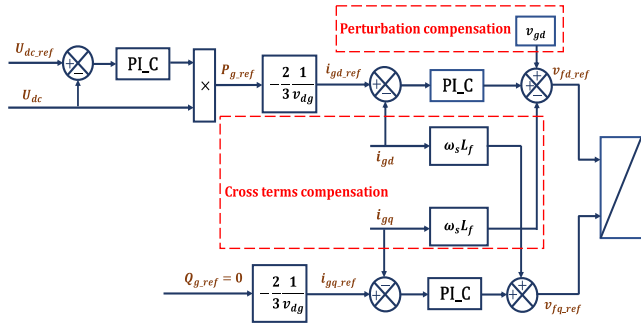
(32)

FIGURE 13. Block diagram of the control strategy for the GSPC.

imposed in order to track a given reference value. To this end, the control input does not act directly on the battery current. Therefore, the control law will be implemented in two steps using the backstepping technique. To begin, let introduce the following error in tracking battery current:

$$z_1 = I_{Bat} - I_{bref} \tag{43}$$

As the battery open circuit voltage U_{ocv} changes at a slower rate than the battery current dynamics. Then it is safe to assume that the time derivation of this latter is neglected. Therefore, using (22)-(23), the time derivation of the battery current tracking error is expressed as follows:

$$\dot{z}_1 = \dot{I}_{bat} - \dot{I}_{bref} = \frac{1}{R_b}\left(\frac{i}{C} - aV_{bat} + aU_{ocv}\right) - \dot{I}_{bref} \tag{44}$$

where: $a = \frac{1}{R_b C}$

According to (44), the quantity $\alpha_1 = ai$ serves as virtual input for the z_1 dynamic. To find a stabilizing function for (44), let Consider the candidate quadratic Lyapunov function $V_1 = 0.5z_1^2$. The time derivation of V_1 along the z_1 trajectory yields:

$$\alpha_1^* = -c_1 z_1 + \frac{a}{R_b}V_{bat} - \frac{a}{R_b}U_{ocv} + \dot{I}_{bref} \tag{45}$$

where $c_1 > 0$ is a design factor. We can't set $\alpha_1 = \alpha_1^*$ because the quantity α_1 isn't the actual command signal. However, the expression of α_1^* is kept as the first stabilizing function, introducing the following tracking error z_2.

$$z_2 = \alpha_1 - \alpha_1^* \tag{46}$$

The dynamic of the z_2 is expressed as follow:

$$\dot{z}_2 = a\left(\mu \frac{V_{dc}}{L} - \frac{V_{bat}}{L}\right) - [-c_1(-c_1 z_1 + z_1)$$
$$+ \frac{a}{R_b}\left(\frac{i}{C} - aV_{bat} + aU_{ocv} + \ddot{I}_{bref}\right)] \tag{47}$$

To analyze the stability of the error system (z_1, z_2), let consider the following augmented Lyapunov function candidate $V_2 = V_1 + 0.5z_2^2$. The time derivation of V_2 along the error

state vector (z_1, z_2) can be made a negative definite function of (z_1, z_2) by:

$$V_2 = z_1\dot{z}_1 + z_2\dot{z}_2 = -c_1^2 z_1 + z_1 z_2 + z_2$$
$$\times \left(ai - \frac{a}{R_b}V_{bat} + \frac{a}{R_b}U_{ocv} + \ddot{I}_{bref}\right) \tag{48}$$

Eq. (47) is easily verified if the command signal is selected as follows:

$$\mu = \frac{L}{aV_{dc}}\left[(c_1^2 - 1)z_1 - (c_1 + c_2)z_2 + a^2 i + \frac{a}{L}V_{bat}\right.$$
$$\left. - \frac{a^2}{R_b}V_{bat} + \frac{a^2}{R_b}U_{ocv}\right] \tag{49}$$

Proposition 1 (Buck Charging Mode): Considering the battery energy storage system described by (21)-(23), in addition to the command law represented by Eq. (40), where c_1 and c_2 are arbitrary positive constants. Then one possesses the following characteristics.

a. In the closed loop, the error system (z_1, z_2) is given by the following equations:

$$\begin{cases} \dot{z}_1 = -c_1 z_1 + z_1 \\ \dot{z}_2 = -c_2 z_2 - z_1 \end{cases} \tag{50}$$

b. With regard to the augmented Lyapunov function $V_2 = 0.5z_1^2 + 0.5z_2^2$, the linear system described by Eq.(50) is globally asymptotically stable. Therefore, the errors system (z_1, z_2) vanish exponentially whatever the initial condition.

2) BOOST DISCHARGING MODE
This mode aims guarantee the safety of the battery during the discharging mode. In this mode, the control objective aims to regulate the output current of the boost converter to help discharging the battery without causing any damage to the battery.

Again, using the backstepping control approach, the control law will be carried out in one step. First, let z_3 denotes the boost converter output current tracking error:

$$z_3 = i - I_{ref} \tag{51}$$

The dynamics of the previous error is expressed as:

$$\dot{z}_3 = \mu \frac{V_{dc}}{L} - \frac{V_{bat}}{L} - \dot{I}_{ref} \tag{52}$$

To analyze the stability in the presence of the error z_3, let chose $V_3 = 0.5z_3^2$ to be the Lyapunov candidate function. The time derivative of V_3 along the error z_3 gives:

$$\dot{V}_3 = z_3\dot{z}_3 = z_3\left(\mu \frac{V_{dc}}{L} - \frac{V_{bat}}{L} - \dot{I}_{ref}\right) \tag{53}$$

It easily to check that the dynamic of V_3 can be made a negative definite function of z_3 by choosing the following control input:

$$\mu = \frac{L}{V_{dc}}\left(-c_3 z_3 + \frac{V_{bat}}{L} + \dot{I}_{ref}\right) \tag{54}$$

where c_3 is a positive design parameter.

Proposition 2 (Boost Mode: Converter Output Current Regulation): Consider the battery energy storage system described by (21)-(23), together with the control law (45), where c_3 is arbitrary positive constant. Then one has the following properties.

a. The closed loop errors system (z_1, z_2) is given by the following equations:

$$\dot{z}_3 = -c_3 z_3 \qquad (55)$$

b. The closed loop error is globally asymptotically stable with respect to the augmented Lyapunov function $V_3 = 0.5 z_3^2$. Therefore, the error z_3 vanish exponentially whatever the initial condition.

E. BATTERY MANAGEMENT ALGORITHM

A battery management algorithm generally is any interface that can manages a rechargeable battery, which is used to optimize the performance and lifespan of a battery, while ensuring its safety and reliability. The proposed algorithm, depicted by the chart-flow in Figure 14, requires continuously the available wind power and the grid nominal power, to establish a smooth switching between the operating modes during any weather conditions.
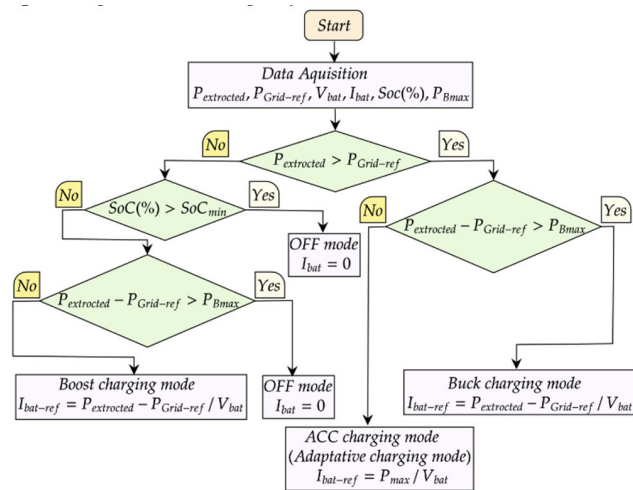
FIGURE 14. Battery management algorithm.

IV. SIMULATION RESULTS AND DISCUSSIONS

This section deals with the performance evaluation of the wind energy conversion system (WECS), equipped with the energy storage system and the MPPT technique with intelligently controlled rotor speed. In the MATLAB / SIMULINK environment, a series of simulations were run using the model of a wind energy conversion chain based on a 1.5 MW DFIG. The simulation parameters of the studied whole system are mentioned in Table 3 in the Appendix.

During the simulation process of the studied global system, we used an extract of a real wind speed of Tetouan city located in the western Rif of the Moroccan country, which

is presented in Figure 15. This last varies between 4 m/s and 12 m/s.

Figure 16 depicts The TSR of the turbine. According to this figure, the turbine's λ is variable and corresponds to the shape of the wind speed. Additionally, the maximum and minimum tip speed ratio TSR is about $\lambda_{max} = 8.45$ and $\lambda_{min} = 8.05$ respectively.

The power coefficient $(C_p (\lambda, \beta))$ is illustrated in Figure 17. From this figure, it is noticed that this coefficientis approximately variable and its optimum value reach to $C_p (\lambda, \beta)\_{max} = 0.377$ for $\beta = 0°$.

Figure 18 describes the mechanical speed of the doubly fed induction generator. It takes the same form as the wind speed profile. Additionally, it is noticed very clearly that we have obtained the two operating modes in the vicinity of the
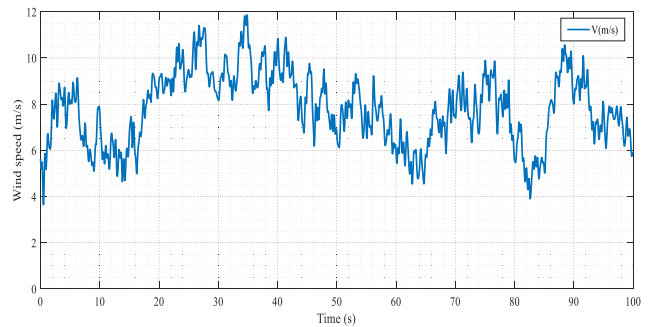

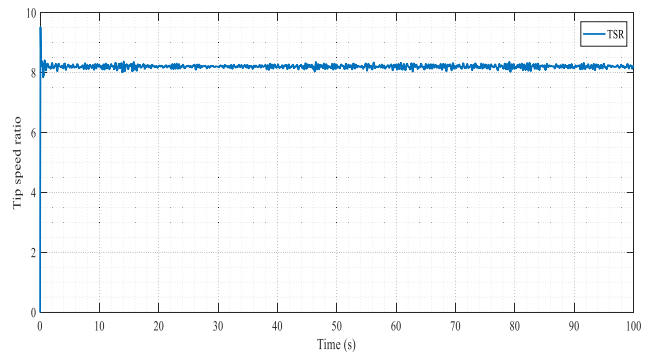**FIGURE 15.** Wind speed of the city of Tetouan.
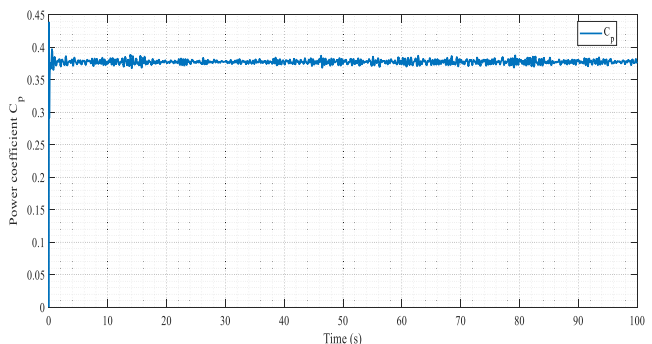

FIGURE 16. Tip speed ration.

FIGURE 17. Power coefficient.
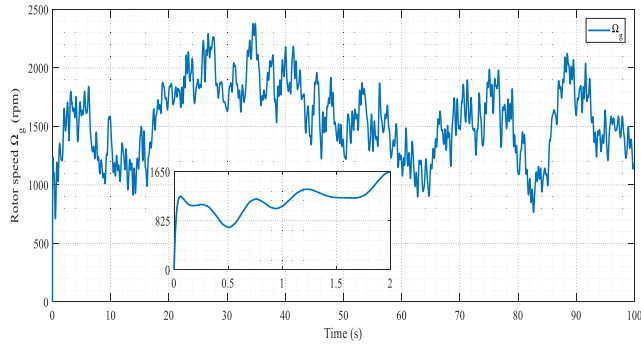
FIGURE 18. Mechanical rotor speed of the DFIG.

FIGURE 20. Generator current i_{rd}.

critical point (the synchronous speed): the hyper-synchronous mode ($\Omega_g > 1500\ rpm$) and the hypo-synchronous mode ($\Omega_g < 1500\ rpm$).

Figures 19-20 show the quadrature and the direct rotor currents of the DFIG. The generator quadrature current i_{rq} fluctuates between a maximum value of $i_{rqmax} = -25.08A$ and a minimum value of $i_{rqmin} = -1467A$, and the generator direct current i_{rd} has a constant value and is almost equal to $i_{rd} = 109A$. Thus, we observe that the shapes of the generator currents i_{rq} and i_{rd} respectively have a relationship with the active P_s and reactive Q_s stator powers. This shows that we have succeeded in achieving a very good decoupling of current axes of our generator.

FIGURE 21. Stator active power P_S.

FIGURE 19. Generator current i_{rq}.

FIGURE 22. Stator reactive power Q_S.

The active P_s and reactive Q_s generated powers are presented in Figures 21–22, respectively. According to these two curves, it is noted that the value of the active stator power P_s decreases with the decrease in the generator quadrature current i_{rq} as well as with the wind speed profile and vice versa, and its value ranges from $P_{smin} = 0.1\ MW$ to $P_{smax} = 1.45\ MW$. On the other hand, the reactive stator power Q_s perfectly follows its null reference that we have chosen ($Q_s^* = 0$) so as to have a better power factor.

The electromagnetic torque T_{em} of the DFIG is displayed in Figure 23. It is worth noting that the active stator power P_s and the electromagnetic torque T_{em} behave similarly. Which confirm that the electromagnetic torque is a reflection of
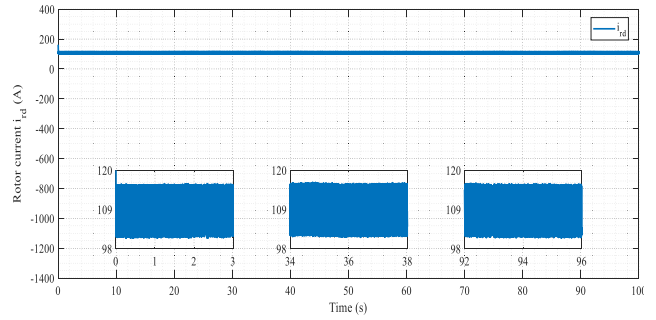

FIGURE 23. Electromagnetic torque.
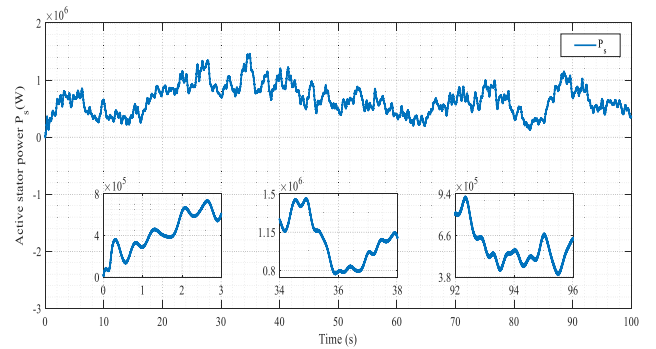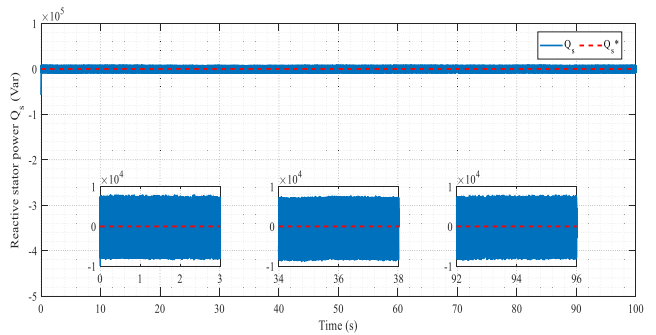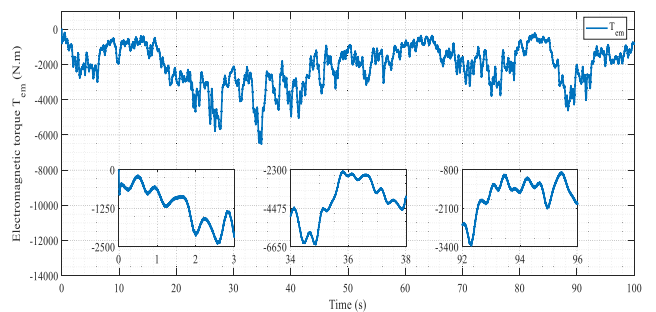
the active stator power, and its value varies from $T_{em\_min} = 240\ N.m$ to $T_{em\_max} = 6625\ N.m$.
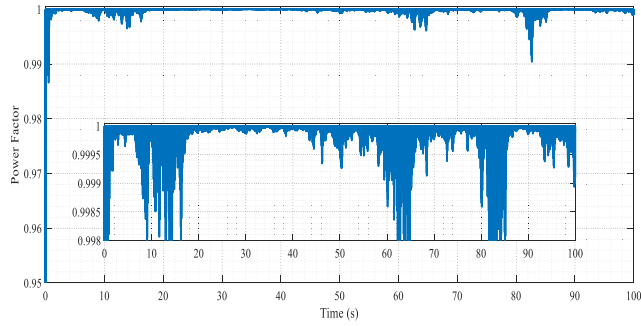
FIGURE 24. Power factor.

As presented in Figure 24, the value of the power factor of the Generator is close to 1 with some remarkable fluctuations in the time intervals $8 \leqslant x \leqslant 18$ s, $50 \leqslant x \leqslant 57$ s and $80 \leqslant x \leqslant 86$ s, which is owing to the fluctuating wind speed and also to the variation of the internal parameters of the generator. In relation, it is important to note that the operation with a unitary power factor is necessary to optimize the quality of the power injected in the grid.

From Figure 25, it can be seen that the DC-link voltage V_{dc} shows fast and precise dynamics. The voltage V_{dc} reaches the reference value of $V_{dc}^* = 1200$ V without overshoot, the static error is then zero once the steady state is reached.
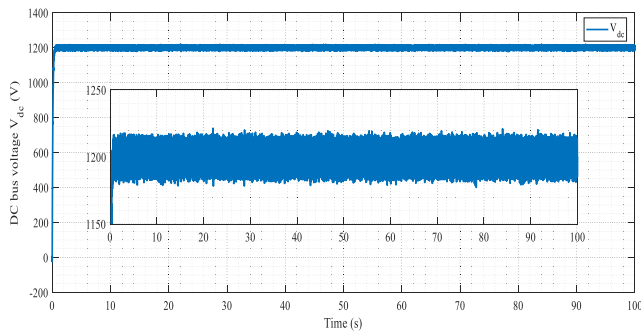
FIGURE 25. Dc bus voltage.

The behavior of the stator and rotor three-phase currents are plotted respectively in Figure 26 and 27. From these two curves, the stator and rotor three-phase currents are sinusoidal, and their magnitudes vary proportionally with the mechanical speed. As the mechanical speed decreases, the values of the currents I_{sabc} and I_{rabc} generated by the DFIG decrease and vice versa. On the other hand, we note that the stator currents have a stable frequency of $f_s = 50$ Hz despite the important fluctuations in the wind speed.

The spectral analysis of the stator current for the phase "a" I_{sa} is shown in Figure 28. According to this figure we have obtained a THD value of 1.33 % (adhere to the IEEE-519 Std). This low THD value reflects the good quality of the stator currents when our proposed robust control is adopted.

To validate the originality of our work, a comparative study with other recently published works is necessary. This comparative study is illustrated in Table 2. Through this comparison, the proposed approach clearly provided us better results
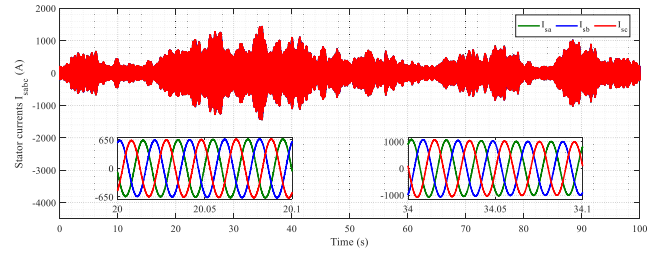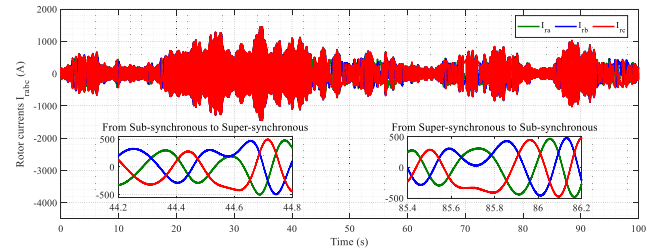

FIGURE 26. Stator currents i_{sabc}.

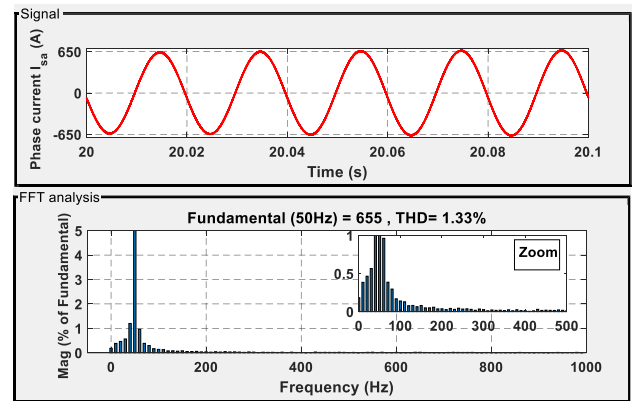**FIGURE 27.** Rotor current i_{rabc}.

FIGURE 28. THD for the stator current i_{sa}.

in terms of response time, static error, overshoot and THD stator currents than some methods performed in recently published works such as the DPC, FOC, Backstepping and Fuzzy SMC strategies.

Figure 29 shows the active power supplied to the grid by the whole WECS based on DFIG (wind turbine + storage system). It is kept almost stable at a value of 0.8 MW. We can see that the active power supplied to the grid is kept equal to 0.8 MW, thanks to the presence of the storage system. Effectively, if we look at the moments when the wind is weak, we see that the power produced by the generator is less than 0.8 MW. It is therefore the storage unit that compensates for this lack of power. Without the storage system, the power supplied to the grid could not have been kept stable over the entire operating time. It is only useful for about half of the time. During the other half of the time it is not useful but it is recharged by using the excess power of the wind. If we had installed a wind turbine without storage system to have

TABLE 2. Comparison of the proposed control method to other recently published works.

References	Methods	Static error (%)	THD i_{sa}(%)	Response time (s)	Overshoot (%)
S. Mensou et al. (2020) [79]	Backstepping	0.29	4.52	0.16	Medium (≈9%)
W.Ayrir et al. (2018) [80]	Fuzzy SMC	0.19	3.1	0.059	Neglected (≈6%)
H. Chojaa et al. (2022) [58]	Classical DPC	0.32	2.62	0.401	Important (≈18%)
E. Chetouani et al. (2022)[84]	HLRNN	0.16	----	0.0018	Important (≈24%)
Proposed method	ISMC	0.157	1.33	0.0017	Neglected (≈5%)
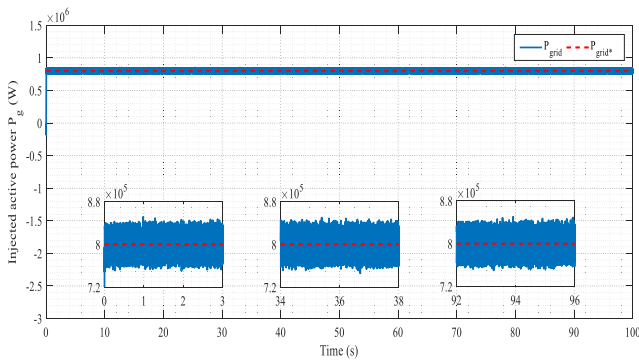
FIGURE 29. Active power supplied to the grid P_g.

0.8 MW to the grid, during the periods of strong wind we would have produced only 0.8 Mw whereas, with the storage unit, we store the power which would not have been exploited to restore it later.

Figure 30 describes the reactive power injected to the grid by the whole system. Here, we have set a null reference ($Q_g^* = 0\ VAR$).
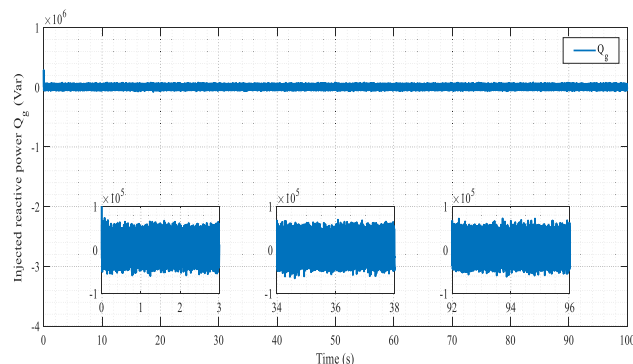

FIGURE 30. Reactive power supplied to the grid Q_g.

Figure 31 corresponds to the storage system power P_B. This power can be positive or negative depending on the wind
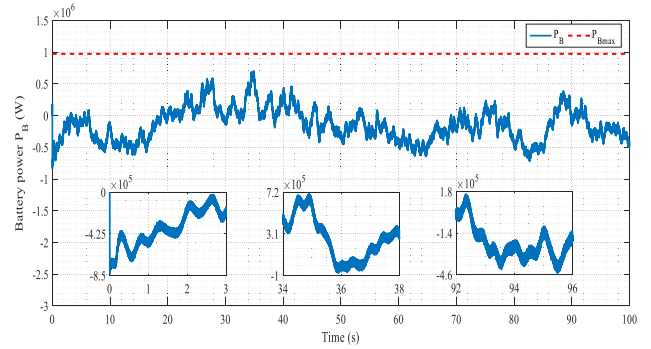

FIGURE 31. Battery Power P_B and its maximum P_{Bmax}.

conditions that allow the charge or discharge of the battery. The storage power is limited to $P_{Bmax} = 1MW$. It is noted that the shape of the power curve of the storage unit P_B varies in the same way as the curve of the generated power P_s, which means that the difference between the generated power Ps and the power of the storage unit is constant to guarantee a stable power supplied to the grid. This means that, in cases where the power generated P_s is greater than 0.8 MW (the power injected to the grid), the storage unit is charged by the rest of the power generated that we don't exploit. On the other hand, in cases where the power generated P_s is less than 0.8 MW (the power injected into the grid), the storage unit discharges so as to provide the remaining power to the grid.

Figures 32-33 illustrate respectively the current and the voltage of the storage system. From these two figures we can see very clearly that these magnitudes vary in the same way as the curve of the power of the storage system. The current of the storage system varies throughout the simulation between a minimum value of $I_{bat\_min} = -1000\ A$ and a maximum value of $I_{bat\_max} = 750\ A$, as long as the voltage of the storage system fluctuates between a maximum value of $V_{bat\_max} = 900\ V$ and a minimum value of $V_{bat\_min} = 663\ V$.
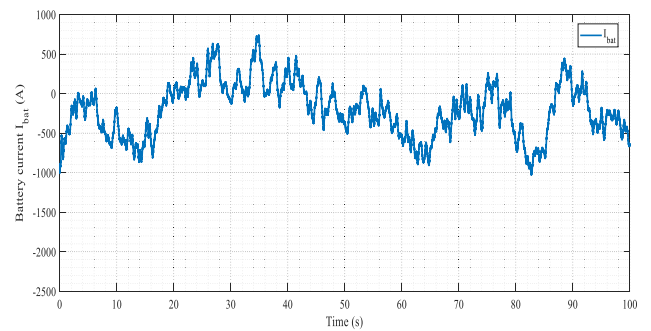

FIGURE 32. Battery current I_{bat}.

Figure 34 describes the percentage of the state of charge of the storage system. From this figure we can see that the state of charge SOC (%) of the storage system decreases progressively in the simulation periods [0; 18s], [43, 61s] and [92; 94.5s], which means that the storage system provides a
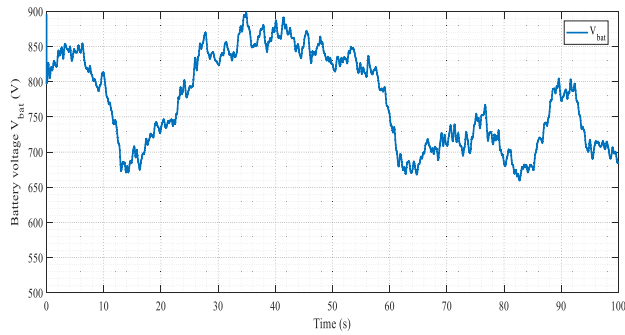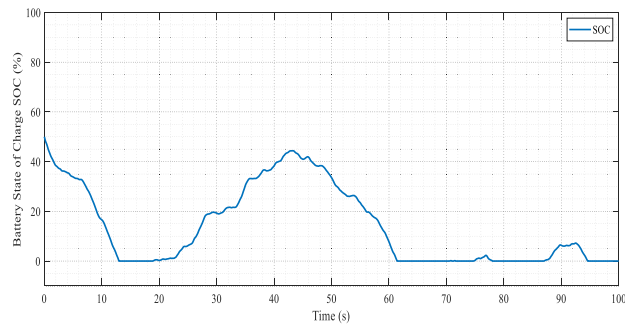
FIGURE 33. Battery voltage V_bat.

FIGURE 35. Stored energy W_stored (Wh).

FIGURE 34. Battery state of charge SOC (%).

FIGURE 36. Balance of grid current and voltage.

power difference between the power produced by the generator and the power that we want to inject into the electrical grid. We also note that in the periods mentioned above, the wind speed is insufficient to produce a power of 0.8 MW to inject it to the grid, while our storage system contributes to maintain a constant power that is supplied to the grid. On the other hand, in the simulation periods [20, 43s] and [88; 93s], the state of charge SOC (%) of the storage system increases progressively, which means that the storage system store the generated power that would not have been exploited to restore it later, in other words, that we are in periods of high wind speed. This energy storage associated with an adequate management would guarantee a constant production throughout the year for the wind farms. This would facilitate their insertion in the networks and would relieve the network managers. Without the storage system, the power supplied to the network could not be maintained throughout the entire operation. It is useful about half the time. For the other half of the time, it is not useful but it is recharged by using the excess power from the wind.

Figure 35 describes the evolution of the energy in the storage system. Itincreases when the wind speed profile is high and decreases during low wind speed profile periods. We notice that the curve varies over several periods without missing energy, because we have chosen the power according to the wind profile. It allows us to feed the grid with a constant power of 0.8MW with a real wind speed profile of Tetouan city. Since the curve represents the energy variation of the storage unit, the sign of this energy is not important because
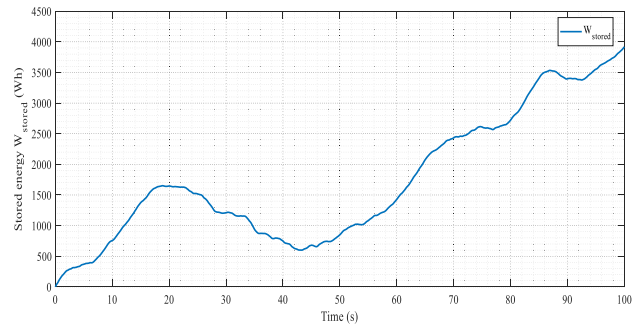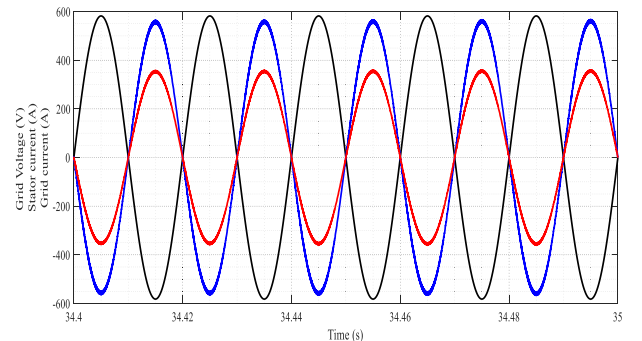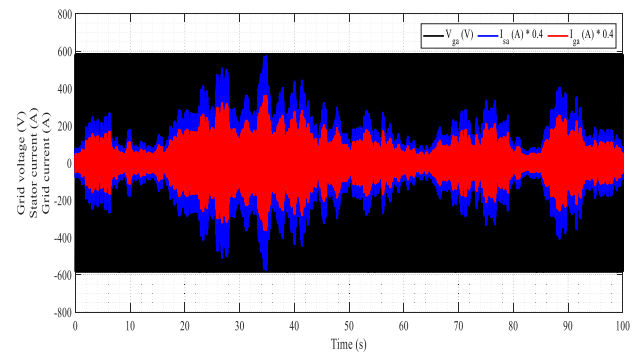
the ordinate at the origin of this curve depends on when we start the calculations. What is important is the variation of the energy.

Figure 36 depicts the grid voltage and current balance of phase "a". The phase opposition of currents with respect to voltage is clearly visible, indicating that the unity power factor is maintained (Qs=0).

V. CONCLUSION

Our research paper enabled us to carry out a comprehensive and global modeling of a wind energy generation system. This modeling is distinguished primarily by the different approach taken by the mechanical part, which relies on aerodynamic calculations to determine the relationships between wind speed, torque, and propeller speed, but also by the study of the whole structure with the association of the storage unit, allowing the supply of constant power to the grid. All of this

has been designed around a DFIG and an intelligent MPPT control based on artificial neural network of the wind turbine in order to maximize the power produced at any given time. The robust integral sliding mode control has investigated to achieve the independent control of active and reactive powers.

The storage unit's implementation and simulation demonstrated that it was prudent to use this solution in order to obtain more convenient production system for the network manager, who can now rely on a constant power as demonstrated by the simulation over a long period. The DFIG produces the maximum amount of wind power available, thanks to the MPPT control, and the storage unit manages its power and energy to keep the power supplied to the grid constant by discharging and recharging itself according to the wind variations. Our WECS, in comparison to a wind turbine without storage, primarily provides a constant power supply to the grid. This is an intriguing aspect because, for a wind turbine without storage, we cannot rely on power all year, and fluctuations in power supplied to the grid are difficult to manage and cause disruptions for users.

We have thus tackled a subject which is in full development, the control of DFIG for wind production is topical and already used in the large commercialized wind turbines. This topic is new in our laboratory and we are happy to have been able to achieve, at the end of these two years of research, a model of an assembly with conclusive results that can be used to continue the tests and consider other operations and compare with other types of generators. We also hope to be able to use these results to realize a test bench in order to validate the simulations and to allow the real operation of a small wind turbine with storage in order to carry out further tests.

Because of the multiplicity of wind turbines connected to the grid and the increasingly important part of the energy produced by wind turbines, new constraints are imposed on them in order to allow compatibility with the grid and thus ensure a most stable operation of the grid. These constraints can be the resistance to voltage dips so that the wind turbine would not disconnect from the grid if a fleeting variation in voltage appears at the point of connection. Fault tolerance is an aspect of reliability, maintaining production if faults appear on the grid. This tolerance allows generation to be maintained while the protection systems isolate the faulty portion of the grid. The possibility of islanding operation is then required in some cases so that the wind turbine can provide power to users when the grid is faulty. All these constraints require studies that should bring solutions to make the insertion of wind turbines in the electrical grid even easier in order to produce a clean and sustainable energy.

APPENDIX

See Table 3.

REFERENCES

[1] O. Ogunrinde, E. Shittu, and K. K. Dhanda, "Investing in renewable energy: Reconciling regional policy with renewable energy growth," *IEEE Eng. Manag. Rev.*, vol. 46, no. 4, pp. 103–111, Dec. 2018, doi: 10.1109/EMR.2018.2880445.

[2] Z. Shi, W. Wang, Y. Huang, P. Li, and L. Dong, "Simultaneous optimization of renewable energy and energy storage capacity with the hierarchical control," *CSEE J. Power Energy Syst.*, vol. 8, no. 1, pp. 95–104, Jan. 2022, doi: 10.17775/CSEEJPES.2019.01470.

[3] S. A. Nabavi, N. H. Motlagh, M. A. Zaidan, A. Aslani, and B. Zakeri, "Deep learning in energy modeling: Application in smart buildings with distributed energy generation," *IEEE Access*, vol. 9, pp. 125439–125461, 2021, doi: 10.1109/ACCESS.2021.3110960.

[4] S. Ganesan, U. Subramaniam, A. A. Ghodke, R. M. Elavarasan, K. Raju, and M. S. Bhaskar, "Investigation on sizing of voltage source for a battery energy storage system in microgrid with renewable energy sources," *IEEE Access*, vol. 8, pp. 188861–188874, 2020, doi: 10.1109/ACCESS.2020.3030729.

[5] M. A. Mossa, O. Gam, N. Bianchi, and N. V. Quynh, "Enhanced control and power management for a renewable energy-based water pumping system," *IEEE Access*, vol. 10, pp. 36028–36056, 2022, doi: 10.1109/ACCESS.2022.3163530.

[6] M. A. Mossa, O. Gam, and N. Bianchi, "Performance enhancement of a hybrid renewable energy system accompanied with energy storage unit using effective control system," *Int. J. Robot. Control. Syst.*, vol. 2, no. 1, pp. 140–171, 2022.

[7] M. Hedayati-Mehdiabadi, J. Zhang, and K. W. Hedman, "Wind power dispatch margin for flexible energy and reserve scheduling with increased wind generation," *IEEE Trans. Sustain. Energy*, vol. 6, no. 4, pp. 1543–1552, Oct. 2015, doi: 10.1109/TSTE.2015.2455552.

[8] J. Xie, X. Zhang, S. Huang, F. Huang, Z. Peng, Y. Dai, and X. Wu, "Characteristics simulation method of megawatt three-blade horizontal axis wind turbine based on laboratory kilowatt low-power motor system," *IEEE Trans. Ind. Appl.*, vol. 58, no. 1, pp. 645–655, Jan. 2022, doi: 10.1109/TIA.2021.3123116.

[9] I. M. Albuquerque and F. F. S. Matos, "A characterization of vertical axis wind turbines," *IEEE Latin Amer. Trans.*, vol. 14, no. 10, pp. 4255–4260, Oct. 2016, doi: 10.1109/TLA.2016.7786302.

[10] J. Y. Jin, M. S. Virk, Q. Hu, and X. Jiang, "Study of ice accretion on horizontal axis wind turbine blade using 2D and 3D numerical approach," *IEEE Access*, vol. 8, pp. 166236–166245, 2020, doi: 10.1109/ACCESS.2020.3022458.

[11] B. Kelkoul and A. Boumediene, "Stability analysis and study between classical sliding mode control (SMC) and super twisting algorithm (STA) for doubly fed induction generator (DFIG) under wind turbine," *Energy*, vol. 214, Jan. 2021, Art. no. 118871, doi: 10.1016/j.energy.2020.118871.

[12] M. H. Mohamed, "Impacts of solidity and hybrid system in small wind turbines performance," *Energy*, vol. 57, pp. 495–504, Aug. 2013, doi: 10.1016/j.energy.2013.06.004.

[13] O. Beik and A. S. Al-Adsani, "Active and passive control of a dual rotor wind turbine generator for DC grids," *IEEE Access*, vol. 9, pp. 1987–1995, 2021, doi: 10.1109/ACCESS.2020.3047267.

[14] S. Nugroho, L. Diana, J. Pratilastiarso, W. A. Giarnayoga, and D. P. Ariyanti, "Computational performance and aerodynamic analysis of multisage wind turbin with dual rotor," in *Proc. Int. Conf. Appl. Sci. Technol. (iCAST)*, Oct. 2018, pp. 607–612, doi: 10.1109/iCAST1.2018.8751265.

TABLE 3. Parameters of Simulink model.

Parameters	Value	Parameters	Value
Number of blades	3	Stator rated frequency, f_s (Hz)	50
Rotor radius R (m)	35.25	Stator resistance, R_s (Ω)	0.012
Gearbox gain G	90	Rotor resistance, R_r (Ω)	0.021
Friction coefficient f (N.m.s/rad)	0.0024	Stator inductance, L_s (H)	0.0137
Moment of inertia J (kg.m²)	1000	Rotor Inductance, L_r (H)	0.0136
Rated power, P_n (MW)	1.5	DC- bus capacitor, C (F)	8×10^{-3}
Stator rated voltage, V_s (V)	698	DC-bus voltage V_{dc} (V)	1200
Number of pair of poles, p	2	filter resistance R_F (Ω)	0.012
Mutual inductance, M (H)	0.0135	Filter inductance L_f (H)	0.005

[15] M. S. Islam, S. M. T. Hoque, M. R. Hazari, M. M. Hasan, and M. Uddin, "Design and simulation of a dual rotor wind turbine based PMSG system," in *Proc. 2nd Int. Conf. Robot., Electr. Signal Process. Techn. (ICREST)*, Jan. 2021, pp. 17–20, doi: 10.1109/ICREST51555.2021.9331134.

[16] M. S. Davis, A. Jafarian, F. Ferdowsi, and M. R. Madani, "Wind energy harvesting capability of a novel cascaded dual-rotor horizontal-axis wind turbine," in *Proc. Int. Conf. Electr., Comput., Commun. Mechatronics Eng. (ICECCME)*, Oct. 2021, pp. 1–51, doi: 10.1109/ICECCME52200.2021.9590963.

[17] M. A. Bramantya and L. A. Huda, "An experimental study on the mechanics power of counter rotating wind turbines model related with axial distance between two rotors," in *Proc. 6th Int. Annu. Eng. Seminar (InAES)*, Aug. 2016, pp. 212–217, doi: 10.1109/INAES.2016.7821936.

[18] B. Singh, V. Rajagopal, A. Chandra, and K. Al-Haddad, "Decoupled electronic load controller for asynchronous generator in pico-hydro power generation," in *Proc. 5th Int. Conf. Ind. Inf. Syst.*, Jul. 2010, pp. 490–495, doi: 10.1109/ICIINFS.2010.5578653.

[19] M. A. Mossa, H. Echeikh, N. V. Quynh, and N. Bianchi, "Performance dynamics improvement of a hybrid wind/fuel cell/battery system for stan-dalone operation," *IET Renew. Power Gener.*, vol. 17, no. 2, pp. 349–375, 2022.

[20] Y. Liu, J. Ou, and M. Noe, "A large-scale superconducting DC wind generator considering concentrated/distributed armature winding," *IEEE Trans. Appl. Supercond.*, vol. 27, no. 4, pp. 1–5, Jun. 2017, doi: 10.1109/TASC.2016.2639026.

[21] J. Ma, D. Zhao, L. Yao, M. Qian, K. Yamashita, and L. Zhu, "Analysis on application of a current-source based DFIG wind generator model," *CSEE J. Power Energy Syst.*, vol. 4, no. 3, pp. 352–361, Sep. 2018, doi: 10.17775/CSEEJPES.2018.00060.

[22] M. A. Mossa, H. Echeikh, and A. Iqbal, "Enhanced control technique for a sensor-less wind driven doubly fed induction generator for energy conversion purpose," *Energy Rep.*, vol. 7, pp. 5815–5833, Nov. 2021, doi: 10.1016/j.egyr.2021.08.183.

[23] M. A. Mossa, H. Echeikh, A. A. Z. Diab, and N. V. Quynh, "Effective direct power control for a sensor-less doubly fed induction generator with a losses minimization criterion," *Electronics*, vol. 9, no. 8, p. 1269, 2020, doi: 10.3390/electronics9081269.

[24] S. Mondal and D. Kastha, "Input reactive power controller with a novel active damping strategy for a matrix converter fed direct torque con-trolled DFIG for wind power generation," *IEEE J. Emerg. Sel. Top-ics Power Electron.*, vol. 8, no. 4, pp. 3700–3711, Dec. 2020, doi: 10.1109/JESTPE.2019.2938012.

[25] K. Xiahou, M. S. Li, Y. Liu, and Q. H. Wu, "Sensor fault tolerance enhancement of DFIG-WTs via perturbation observer-based DPC and two-stage Kalman filters," *IEEE Trans. Energy Convers.*, vol. 33, no. 2, pp. 483–495, Jun. 2018, doi: 10.1109/TEC.2017.2771250.

[26] S. S. Yu, G. Zhang, T. Fernando, and H. H.-C. Iu, "A DSE-based SMC method of sensorless DFIG wind turbines connected to power grids for energy extraction and power quality enhancement," *IEEE Access*, vol. 6, pp. 76596–76605, 2018, doi: 10.1109/ACCESS.2018.2883591.

[27] A. Ardjal, M. Bettayeb, and R. Mansouri, "Fractional nonlinear synergetic control of wind turbine for maximum power point tracking," in *Proc. IEEE Int. Symp. Signal Process. Inf. Technol. (ISSPIT)*, Dec. 2019, pp. 1–6, doi: 10.1109/ISSPIT47144.2019.9001862.

[28] X. Wang, D. Sun, and Z. Q. Zhu, "Resonant-based backstepping direct power control strategy for DFIG under both balanced and unbalanced grid conditions," *IEEE Trans. Ind. Appl.*, vol. 53, no. 5, pp. 4821–4830, Sep. 2017, doi: 10.1109/TIA.2017.2700280.

[29] P. Li, L. Xiong, Z. Wang, M. Ma, and J. Wang, "Fractional-order sliding mode control for damping of subsynchronous control interaction in DFIG-based wind farms," *Wind Energy*, vol. 23, no. 3, pp. 749–762, 2020, doi: 10.1002/we.2455.

[30] L. Xiong, P. Li, and J. Wang, "High-order sliding mode control of DFIG under unbalanced grid voltage conditions," *Int. J. Elect. Power Energy Syst.*, vol. 117, May 2020, Art. no. 105608, doi: 10.1016/j.ijepes.2019.105608.

[31] H. Xue, Y. Wang, and F. Yang, "Adaptive passivity-based control strategies of doubly fed induction wind power generator systems," in *Proc. 2nd Int. Symp. Power Electron. Distrib. Gener. Syst.*, Jun. 2010, pp. 731–734, doi: 10.1109/PEDG.2010.5545935.

[32] N. Rezaei, M. N. Uddin, I. K. Amin, M. L. Othman, and M. Marsadek, "Genetic algorithm-based optimization of overcurrent relay coordina-tion for improved protection of DFIG operated wind farms," *IEEE Trans. Ind. Appl.*, vol. 55, no. 6, pp. 5727–5736, Nov. 2019, doi: 10.1109/TIA.2019.2939244.

[33] X. Zheng and X. Chen, "Enhancement on transient stability of LVRT of DFIG based on neural network D-STATCOM and crowbar," in *Proc. 11th IEEE Int. Conf. Anti-Counterfeiting, Secur., Identificat. (ASID)*, Oct. 2017, pp. 64–68, doi: 10.1109/ICASID.2017.8285745.

[34] M. T. Hagh, S. Roozbehani, F. Najaty, S. Ghaemi, Y. Tan, and K. M. Muttaqi, "Direct power control of DFIG based wind turbine based on wind speed estimation and particle swarm optimization," in *Proc. Australas. Universities Power Eng. Conf. (AUPEC)*, Sep. 2015, pp. 1–6, doi: 10.1109/AUPEC.2015.7324889.

[35] K. Belmokhtar, M. L. Doumbia, and K. Agbossou, "Modelling and fuzzy logic control of DFIG based wind energy conversion systems," in *Proc. IEEE Int. Symp. Ind. Electron.*, May 2012, pp. 1888–1893, doi: 10.1109/ISIE.2012.6237380.

[36] H. Benbouhenni, F. Mehedi, and L. Soufiane, "New direct power synergetic-SMC technique based PWM for DFIG integrated to a variable speed dual-rotor wind power," *Automatika*, vol. 63, no. 4, pp. 718–731, Dec. 2022, doi: 10.1080/00051144.2022.2065801.

[37] T. K. Roy and M. A. Mahmud, "Hybrid robust adaptive backstepping sliding mode controller design for mitigating SSR in series-compensated DFIG-based wind generation systems," in *Proc. IEEE Ind. Appl. Soc. Annu. Meeting (IAS)*, Oct. 2021, pp. 1–6, doi: 10.1109/IAS48185.2021.9677445.

[38] H. Gasmi, S. Mendaci, S. Laifa, W. Kantas, and H. Benbouhenni, "Frac-tional order proportional integral super-twisting sliding mode controller for wind energy conversion system equipped with doubly fed induc-tion generator," *J. Power Electron.*, vol. 22, no. 8, p. 1357, 2022, doi: 10.1007/s43236-022-00430-0.

[39] L. Djilali, E. N. Sanchez, and M. Belkheiri, "Neural sliding mode field oriented control for DFIG based wind turbine," in *Proc. IEEE Int. Conf. Syst., Man, Cybern. (SMC)*, Oct. 2017, pp. 2087–2092, doi: 10.1109/SMC.2017.8122927.

[40] H. Es-Sarraj, A. E. Bakri, R. M. Alaoui, and I. Boumhidi, "FSMC for PWM rotor side converter in DFIG-based wind turbine system," in *Proc. Int. Conf. Intell. Syst. Comput. Vis. (ISCV)*, May 2022, pp. 1–7, doi: 10.1109/ISCV54655.2022.9806083.

[41] H. Chojaa, A. Derouich, O. Zamzoum, S. Mahfoud, M. Taoussi, H. Albalawi, H. Benbouhenni, and M. I. Mosaad, "A novel DPC approach for DFIG-based variable speed wind power systems using dSPACE," *IEEE Access*, vol. 11, pp. 9493–9510, 2023, doi: 10.1109/ACCESS.2023.3237511.

[42] M. A. Mossa, O. Gam, and N. Bianchi, "Dynamic performance enhance-ment of a renewable energy system for grid connection and stand-alone operation with battery storage," *Energies*, vol. 15, no. 3, p. 1002, 2022, doi: 10.3390/en15031002.

[43] O. Hachana, B. Meghni, A. Benamor, and I. Toumi, "Efficient PMSG wind turbine with energy storage system control based shuffled complex evolution optimizer," *ISA Trans.*, vol. 131, pp. 377–396, Dec. 2022, doi: 10.1016/j.isatra.2022.05.014.

[44] A. Watil, A. E. Magri, A. Raihani, R. Lajouad, F. Giri, "An adaptive nonlinear observer for sensorless wind energy conversion system with PMSG," *Control Eng. Pract.*, vol. 98, May 2020, Art. no. 104356, doi: 10.1016/j.conengprac.2020.104356.

[45] F. Díaz-González, A. Sumper, O. Gomis-Bellmunt, and R. Villafáfila-Robles, "A review of energy storage technologies for wind power applications," *Renew. Sustain. Energy Rev.*, vol. 16, no. 4, pp. 2154–2171, May 2012, doi: 10.1016/j.rser.2012.01.029.

[46] Y. Yang, S. Bremner, C. Menictas, and M. Kay, "Battery energy stor-age system size determination in renewable energy systems: A review," *Renew. Sustain. Energy Rev.*, vol. 91, pp. 109–125, Aug. 2018, doi: 10.1016/j.rser.2018.03.047.

[47] P. H. A. Barra, W. C. D. Carvalho, T. S. Menezes, R. A. S. Fernandes, and D. V. Coury, "A review on wind power smoothing using high-power energy storage systems," *Renew. Sustain. Energy Rev.*, vol. 137, Mar. 2021, Art. no. 110455, doi: 10.1016/j.rser.2020.110455.

[48] K.-Y. Lo, Y.-M. Chen, and Y.-R. Chang, "MPPT battery charger for stand-alone wind power system," *IEEE Trans. Power Electron.*, vol. 26, no. 6, pp. 1631–1638, Jun. 2011, doi: 10.1109/TPEL.2010.2088405.

[49] V. Marano, S. Onori, Y. Guezennec, G. Rizzoni, and N. Madella, "Lithium-ion batteries life estimation for plug-in hybrid electric vehicles," in *Proc. IEEE Vehicle Power Propuls. Conf.*, Sep. 2009, pp. 536–543, doi: 10.1109/VPPC.2009.5289803.

[50] A. Pirooz and R. Noroozian, "Model predictive control of classic bidirectional DC–DC converter for battery applications," in *Proc. 7th Power Electron. Drive Syst. Technol. Conf. (PEDSTC)*, Feb. 2016, pp. 517–522, doi: 10.1109/PEDSTC.2016.7556914.

[51] A. Eddahech, O. Briat, and J.-M. Vinassa, "Neural networks based model and voltage control for lithium polymer batteries," in *Proc. 8th IEEE Symp. Diag. Electr. Mach., Power Electron. Drives*, Sep. 2011, pp. 645–650, doi: 10.1109/DEMPED.2011.6063692.

[52] L. Haoran, L. Liangdong, Z. Xiaoyin, and S. Mingxuan, "Lithium battery SOC estimation based on extended Kalman filtering algorithm," in *Proc. IEEE 4th Int. Conf. Control Sci. Syst. Eng. (ICCSSE)*, Aug. 2018, pp. 231–235, doi: 10.1109/CCSSE.2018.8724766.

[53] E. Purwanto, I. Ferdiansyah, F. H. Sholihah, S. D. Nugraha, O. A. Qudsi, and S. A. Zerlina, "Prevention of battery life reduction using fuzzy logic controller-SEPIC converter for automatic battery charging," in *Proc. Int. Conf. Electr. Inf. Technol. (IEIT)*, Sep. 2022, pp. 267–270, doi: 10.1109/IEIT56384.2022.9967872.

[54] I. Jokic, Ž. Zecevic, and B. Krstajic, "State-of-charge estimation of lithium-ion batteries using extended Kalman filter and unscented Kalman filter," in *Proc. 23rd Int. Sci.-Prof. Conf. Inf. Technol. (IT)*, Feb. 2018, pp. 1–4, doi: 10.1109/SPIT.2018.8350462.

[55] P. K. Anju and P. P. Zarina, "Power fluctuation reduction using battery system in DFIG based wind energy conversion system," in *Proc. Int. Conf. Current Trends Towards Converging Technol. (ICCTCT)*, Mar. 2018, pp. 1–5, doi: 10.1109/ICCTCT.2018.8551053.

[56] S. Yang, S. Li, T. Wang, F. Liang, and X. Su, "A sensorless control strategy of a single-stage fast EV battery charger based on the voltage-type PWM converter," in *Proc. 4th Int. Conf. HVDC (HVDC)*, Nov. 2020, pp. 1055–1059, doi: 10.1109/HVDC50696.2020.9292707.

[57] Q. Yan, "SOC prediction of power battery based on SVM," in *Proc. Chin. Control Decis. Conf. (CCDC)*, Aug. 2020, pp. 2425–2429, doi: 10.1109/CCDC49329.2020.9164245.

[58] H. Chojaa, A. Derouich, S. E. Chehaidia, O. Zamzoum, M. Taoussi, H. Benbouhenni, and S. Mahfoud, "Enhancement of direct power control by using artificial neural network for a doubly fed induction generator-based WECS: An experimental validation," *Electronics*, vol. 11, no. 24, p. 4106, 2022, doi: 10.3390/electronics11244106.

[59] T. Liu, X. Ye, and B. Sun, "Combining convolutional neural network and support vector machine for gait-based gender recognition," in *Proc. Chin. Autom. Congr. (CAC)*, Nov. 2018, pp. 3477–3481, doi: 10.1109/CAC.2018.8623118.

[60] Z. Yu, H.-S. Wong, and G. Wen, "A modified support vector machine and its application to image segmentation," *Image Vis. Comput.*, vol. 29, no. 1, pp. 29–40, 2011, doi: 10.1016/j.imavis.2010.08.003.

[61] M. Banerjee and H. Kaur, "A comparison among lithium-ion, nickel-cadmium & nickel-metal-hydride batteries for charging and discharging in electric vehicle by bidirectional DC–DC converter," in *Proc. IEEE IAS Global Conf. Emerg. Technol. (GlobConET)*, May 2022, pp. 361–368, doi: 10.1109/GlobConET53749.2022.9872335.

[62] C. Hamid, A. Derouich, T. Hallabi, O. Zamzoum, M. Taoussi, S. Rhaili, and O. Boulkhrachef, "Performance improvement of the variable speed wind turbine driving a DFIG using nonlinear control strategies," *Int. J. Power Electron. Drive Syst. (IJPEDS)*, vol. 12, no. 4, p. 2470, Dec. 2021, doi: 10.11591/ijpeds.v12.i4.pp2470-2482.

[63] H. Chojaa, A. Derouich, M. Taoussi, O. Zamzoum, and M. Yessef, "Optimization of DFIG wind turbine power quality through adaptive fuzzy control," in *Digital Technologies and Applications* (Lecture Notes in Networks and Systems), vol. 211. Cham, Switzerland: Springer, 2021, doi: 10.1007/978-3-030-73882-2_113.

[64] M. M. Montazeri and D. Xu, "Coordination of DFIG and STATCOM in a power system," in *Proc. IEEE Int. Symp. Ind. Electron.*, May 2012, pp. 993–998, doi: 10.1109/ISIE.2012.6237224.

[65] X. Zhu, Y. Wang, L. Xu, X. Zhang, and H. Li, "Virtual inertia control of DFIG-based wind turbines for dynamic grid frequency support," in *Proc. IET Conf. Renew. Power Gener. (RPG)*, 2011, pp. 1–6, doi: 10.1049/cp.2011.0189.

[66] W. Tang, J. Hu, Y. Chang, and F. Liu, "Modeling of DFIG-based wind turbine for power system transient response analysis in rotor speed control timescale," *IEEE Trans. Power Syst.*, vol. 33, no. 6, pp. 6795–6805, Nov. 2018, doi: 10.1109/TPWRS.2018.2827402.

[67] H. Chojaa, A. Derouich, M. Taoussi, S. E. Chehaidia, O. Zamzoum, M. I. Mosaad, A. Alhejji, and M. Yessef, "Nonlinear control strategies for enhancing the performance of DFIG-based WECS under a real wind profile," *Energies*, vol. 15, no. 18, p. 6650, 2022, doi: 10.3390/en15186650.

[68] W. Aziz, E. M. Abdelmounime, L. Rachid, R. Abdelhadi, G. Fouad, E. F. Abderrahim, M. Adil, "A power balance control strategy for stand alone wind energy conversion systems," *IFAC-PapersOnLine*, vol. 55, no. 12, pp. 788–793, 2022, doi: 10.1016/j.ifacol.2022.07.409.

[69] S. Abu-Sharkh and D. Doerffel, "Rapid test and non-linear model characterisation of solid-state lithium-ion batteries," *J. Power Sources*, vol. 130, nos. 1–2, pp. 266–274, 2004, doi: 10.1016/j.jpowsour.2003.12.001.

[70] R. Zhong, D. Changqing, Z. Wu, J. Shao, and W. Deng, "A comparative study of the influence of different open circuit voltage tests on model-based state of charge estimation for lithium-ion batteries," *Int. J. Energy Res.*, vol. 45, no. 9, pp. 13692–13711, 2021, doi: 10.1002/er.6700.

[71] T. Riouch and R. El-Bachtiri, "Comparative study of fuzzy logic controller and sliding mode for enhancing the behavior of the DFIG under fault," in *Proc. Int. Conf. Multimedia Comput. Syst. (ICMCS)*, Apr. 2014, pp. 1602–1607, doi: 10.1109/ICMCS.2014.6911241.

[72] A. Susperregui, M. I. Martinez, G. Tapia-Otaegui, and A. Etxeberria, "Sliding-mode control algorithm for DFIG synchronization to unbalanced and harmonically distorted grids," *IEEE Trans. Sustain. Energy*, vol. 13, no. 3, pp. 1566–1579, Jul. 2022, doi: 10.1109/TSTE.2022.3166217.

[73] F. Mazouz, S. Belkacem, S. Drid, L. Chrifi-Alaoui, and I. Colak, "Fuzzy sliding mode control of DFIG applied to the WECS," in *Proc. 8th Int. Conf. Syst. Control (ICSC)*, Oct. 2019, pp. 465–470, doi: 10.1109/ICSC47195.2019.8950675.

[74] K. V. Shihabudheen, G. N. Pillai, and S. K. Raju, "Neuro-fuzzy control of DFIG wind energy system with distribution network," *Electr. Power Compon. Syst.*, vol. 46, no. 13, pp. 1416–1431, Aug. 2018, doi: 10.1080/15325008.2018.1499154.

[75] L. Djilali, A. Badillo-Olvera, Y. Y. Rios, H. López-Beltrán, and L. Saihi, "Neural high order sliding mode control for doubly fed induction generator based wind turbines," *IEEE Latin Amer. Trans.*, vol. 20, no. 2, pp. 223–232, Feb. 2022, doi: 10.1109/TLA.2022.9661461.

[76] M. Karabacak, "A new perturb and observe based higher order sliding mode MPPT control of wind turbines eliminating the rotor inertial effect," *Renew. Energy*, vol. 133, pp. 807–827, Apr. 2019, doi: 10.1016/j.renene.2018.10.079.

[77] R. K. Patnaik, P. K. Dash, and S. P. Mishra, "Adaptive third order terminal sliding mode power control of DFIG based wind farm for power system stabilisation," *Int. J. Dynam. Control*, vol. 8, no. 2, pp. 629–643, 2020, doi: 10.1007/s40435-019-00567-0.

[78] H. Chojaa, A. Derouich, C. S. Eddine, O. Zamzoum, M. Taoussi, and H. Elouatouat, "Integral sliding mode control for DFIG based WECS with MPPT based on artificial neural network under a real wind profile," *Energy Rep.*, vol. 7, pp. 4809–4824, Nov. 2021, doi: 10.1016/j.egyr.2021.07.066.

[79] S. Mensou, A. Essadki, T. Nasser, B. B. Idrissi, and L. B. Tarla, "dSPACE DS1104 implementation of a robust nonlinear controller applied for DFIG driven by wind turbine," *Renew. Energy*, vol. 147, pp. 1759–1771, Mar. 2020, doi: 10.1016/j.renene.2019.09.042.

[80] W. Ayrir, M. Ourahoua, B. E. Hassounia, and A. Haddi, "Direct torque control improvement of a variable speed DFIG based on a fuzzy inference system," *Math. Comput. Simul.*, vol. 167, pp. 308–324, Jan. 2020, doi: 10.1016/j.matcom.2018.05.014.

[81] E. Chetouani, Y. Errami, A. Obbadi, and S. Sahnoun, "Self-adapting PI controller for grid-connected DFIG wind turbines based on recurrent neural network optimization control under unbalanced grid faults," *Electr. Power Syst. Res.*, vol. 214, Jan. 2023, Art. no. 108829, doi: 10.1016/j.epsr.2022.108829.

HAMID CHOJAA was born in Settat, Morocco, in 1990. He received the master's degree in science and technology from Hassan 1er University, in 2014. His master's dissertation titled "Automatic Control, Signal Processing, and Industrial Computing." He is currently working on a doctoral thesis with the Electrical Engineering Department, Higher School of Technology, USMBA University, Fez. His research interests include renewable energy, machine control, and electrical systems.

AZIZ DEROUICH received the Diploma degree from the Superior School of Technical Teaching of Rabat, in 1995, the Diploma of Superior Studies (D.E.S.A.) degree in electronics, automatic and information processing and the Ph.D. degree in computer engineering from Sidi Mohamed Ben Abdellah University, Fez, Morocco, in 2004 and 2011, respectively, and the Diploma of Habilitation Research degree from the Faculty of Science and Technology of Fez, in 2014. He was a Professor in electrical and computer science with Lycée Technique, El Jadida, from 1995 to 1999, and Lycée Technique, Fez, from 1999 to 2011. Since 2011, he has been a Professor with the Higher School of Technology, Sidi Mohamed Ben Abdellah University. His research interests include electrotechnical systems, static converters, electrical machines control, renewable energy, and e-learning.

OTHMANE ZAMZOUM received the degree in mechatronic engineering from the National School of Applied Sciences, Fez, Morocco, and the Ph.D. degree in electrical engineering from the Higher School of Technology, Fez. He was engaged in research and improvement of the electrical machine control in wind turbine application. His current research interests include renewable energy and non-linear control strategies applied on power electronics and machine drives.

AZIZ WATIL is currently pursuing the Ph.D. degree in electrical engineering and control systems with the Hassan II University of Casablanca. He has published several articles in top-tier journals. His research interests include control theory and its application in renewable energy systems, with a particular focus on optimizing control systems for renewable energy generation and integrating them with battery energy storage systems. He has contributed to the advancement of renewable energy integration in the existing power grid.

MOHAMMED TAOUSSI was born in Fez, Morocco. He received the master's degree in industrial electronics from the Faculty of Sciences, Fez, in 2013. He is currently pursuing the Ph.D. degree in electrical engineering from Sidi Mohammed Ben Abdellah University, Faculty of Sciences, Morocco. He is also a Professor with Sidi Mohammed Ben Abdellah University. His research interests include static converters, electrical motor drives, power electronics, smart grids, renewable energy, and artificial intelligence.

ALMOATAZ Y. ABDELAZIZ (Senior Member, IEEE) received the Ph.D. degree in electrical engineering according to the channel system between Ain Shams University and Brunel University, U.K., in 1996. He has been a Professor of electrical power engineering with Ain Shams University, since 2007. He is currently delegated in Faculty of Engineering and Technology, Future University in Egypt, which he was the Vice Dean of education and students affairs from 2018 to 2019. He has authored or coauthored more than 550 refereed journals and conference papers, 45 book chapters, and six edited books with Elsevier, Springer, and CRC Press. In addition, he has supervised more than 80 master's and 40 Ph.D. theses. He is a member in the Egyptian Sub-Committees of IEC and CIGRE. He has been awarded many prizes for distinct researches and for international publishing from Ain Shams University and Future University in Egypt. He is the Chair of the IEEE Education Society Chapter in Egypt. He is an Editor of Electric Power Components and Systems journal. He is an editorial board member, an editor, an associate editor, and an editorial advisory board member for many international journals. His research interests include the applications of artificial intelligence and evolutionary and heuristic optimization techniques to power system planning, operation, and control.

Z. M. S. ELBARBARY was born in Kafr El-Sheikh, Egypt, in 1971. He received the B.Sc., M.Sc., and Ph.D. degrees in electrical engineering from Menoufia University, Egypt, in 1994, 2002, and 2007, respectively. In 2009, he joined Kafrelsheikh University as an Assistant Professor and promoted to a Full Professor in power electronics, in June 2022. In 2016, he was a Research Visitor with Ghent University, Ghent, Belgium, for two months. His research interests include control of electrical machines, senseless control, applications of power electronics, real-time control using digital signals processing, and renewable energy applications.

MAHMOUD A. MOSSA received the bachelor's and master's degrees in electrical engineering from the Faculty of Engineering, Minia University, Egypt, in 2008 and 2013, respectively, and the Ph.D. degree in electrical engineering, in April 2018. Since January 2010, he has been an Assistant Lecturer with the Electrical Engineering Department, Minia University. In November 2014, he joined the Electric Drives Laboratory (EDLAB), University of Padova, Italy, for the Ph.D. research activities. Since May 2018, he has been an Assistant Professor with the Electrical Engineering Department, Minia University. He occupied a postdoctoral fellow position with the Department of Industrial Engineering, University of Padova, in 2021 and 2022. His research interests include electric machine drives, renewable energy systems, power management, optimization, power electronics, and load frequency control.

● ● ●